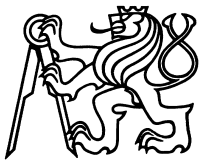

Czech Technical University in Prague
Faculty of Nuclear Sciences and Physical Engineering

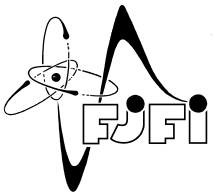

Monte Carlo simulations of radiotherapy treatment with laser accelerated particles

Monte Carlo simulace léčby radioterapií s laserem urychlenými částicemi

Diplomová práce

Author: **Bc. Vanda Sluková**

Supervisor: **MSc. Gabriele Maria Grittani, Ph.D.**

Consultant: **Ing. Michal Nevrkla, Ph.D**

Academic year: 2021/2022

ČESKÉ VYSOKÉ UČENÍ TECHNICKÉ V PRAZE

FAKULTA JADERNÁ A FYZIKÁLNĚ INŽENÝRSKÁ

Katedra fyzikální elektroniky

ZADÁNÍ DIPLOMOVÉ PRÁCE

Student:	**Bc. Vanda S l u k o v á**
Studijní program:	**Fyzikální elektronika**
Specializace:	**Laserová fyzika a technika**
Akademický rok:	**2021/2022**
Název práce: (česky)	**Monte Carlo simulace léčby radioterapií s laserem urychlenými částicemi**
Název práce: (anglicky)	**Monte Carlo simulations of radiotherapy treatment with laser accelerated particles**

Cíl práce:

Cílem práce je vylepšit a optimalizovat ozařovací plán pro laserem řízenou VHEE radioterapii. Porovnat další přístupy radioterapie a připravit experimentální soustavu.

Pokyny pro vypracování:

1. Nastudujte fyzikální aspekty laserového plazmového urychlování
2. Proveďte rešerši nynějšího stavu radioterapie využívající elektrony s velkou energií (VHEE)
3. Nasimulujte transport záření od zdroje k pacientovi ve zjednodušené geometrií
4. Nasimulujte léčbu radioterapií v realistické konfiguraci
5. Připravte experimentální soustavu pro testy spojené s technologickým vývojem v ELI-Beamlines

Doporučená literatura:

1. Salehi F., Le M., Railing L., Kolesik M., Milchberg H. M., Laser-accelerated, low-divergence 15-MeV quasimonoenergetic electron bunches at 1 kHz, Phys. Rev., 11, 2021.
2. Maier R., Delbos N. M., Eichner T., Hübner L., Jalas S., Jeppe L., Jolly S. W., Kirchen M., Leroux V., Messner P., Schnepp M., Trunk M., Walker P. A., Werle C., Winkler P., Decoding Sources of Energy Variability in a Laser-Plasma Accelerator, Phys. Rev., 10, 2020.
3. Thaury, Guilliaume E., Lifschitz A., Ta Phuoc K., Hansson M., Grittani G., Gautier J., Goddet J. P., Tafzi A., Lundh O., Malka V., Shock assisted ionization injection in laser plasma accelerators, Scientific Reports, 5, 2015.
4. Fuchs T., Szymanowski H., Oelfke U., Glinec Y., Rechatin C., Faure J., Malka V., Treatment planning for laser-accelerated very-high energy electrons, Phys. Med. Biol., 54(11), 2009.
5. Bazalova-Carter M., Qu B., Palma B., Hårdemark B., and Hynning E., Jensen Ch., Maxim P. G., and Loo B. W., Jr., Treatment planning for radiotherapy with very high-energy electron beams and comparison of VHEE and VMAT plans, Medical Physics, 42(5), 2015.
6. Palma B., Bazalova-Carter M., Hardemark B., Hynning E., Qu B., Loo W.Jr., Maxim P. G., Assessment of the quality of very high-energy electron radiotherapy planning, Radiother. Oncol., 119(1), 2016.
7. Subiel, Moskvin V., Welsh G. H., Cipiccia S., Reboredo D., DesRosiers C., Jaroszynski D. A., Chalanges of dosimetry of ultra-short pulsed very high energy electron beams, Physica Medica, 76, 2020.

Jméno a pracoviště vedoucího práce:

MSc. Gabriele Maria Grittani, Ph.D.
Fyzikální ústav AV ČR, v. v. i.

Jméno a pracoviště konzultanta:

Ing. Michal Nevrkla, Ph.D.
Katedra fyzikální elektroniky, Fakulta jaderná a fyzikálně inženýrská ČVUT v Praze

Datum zadání: 15. říjen 2021

Datum odevzdání: 2. květen 2022

Doba platnosti zadání je dva roky od data zadání.

.....

Garant programu

.....

Vedoucí katedry

.....

Děkan

V Praze dne 15.10.2021

Acknowledgment:
I would like to thank MSc. Gabriele Maria Grittani, Ph.D. for his expert guidance and express my gratitude to Mgr. Illia Zymak, Ph.D., Ing. Michal Nevrkla, Ph.D, Dávid Horváth, MSc. Carlo Maria Lazzarini, Ing. Lukáš Knybel, PhD, doc. MUDr. Ing. Jakub Cvek, PhD, MBA and MSc. Dr Marco Favetta for their support and advice.

Author's declaration:
I declare that this Diploma thesis is entirely my own work and I have listed all used sources in the bibliography.

Prague, May 2, 2022 Bc. Vanda Sluková

Název práce:

Monte Carlo simulace léčby radioterapií s laserem urychlenými částicemi

Autor: Bc. Vanda Sluková

Obor: Fyzikální elektronika

Zaměření: Laserová fyzika a technika

Druh práce: Diplomová práce

Vedoucí práce: MSc. Gabriele Maria Grittani, Ph.D.
Fyzikální ústav AV ČR, v.v.i

Konzultant: Ing. Michal Nevrkla, Ph.D.
Katedra fyzikální elektroniky, Fakulta jaderná a fyzikálně inženýrská ČVUT v Praze

*Abstrakt:*Tato práce se zaměřuje na využití laserového plazmového urychlovače ke generaci velmi vysoce energetických elektronů (VHEE) a dalších částic pro radioterapii. S využitím obecně účelového Monte Carlo kódu FLUKA a jeho grafického rozhraní Flair byl proveden léčebný plán reálného mozkového nádoru ve zjednodušené geometrii a s reálným léčebným přístrojem. Geometrie přístroje je založená na technickém návrhu laserem řízeného radioterapeutického přístroje navrženého v ELI Beamlines. V této práci jsou svazky záření optimalizované ve smyslu geometrie (polohy okolo pacienta) a čas léčby je vypočítán. Různé kombinace parametrů jsou zkoumány a příslušné časy jsou vypočítány. Plánování léčby je také zkoumáno pro pozitronové svazky. Skrz touto prací se pracuje hlavně s tužkovým skenováním (PBS) a proto pro srovnání použití vícelamelového kolimátoru je zkoumáno. Dále následuje představení experimentu a s ním spojených simulací provedených v ELI Beamlines týmem zabývajícím se urychlovaní elektronů.

Klíčová slova: interakce záření s hmotou, laserové urychlování brázdového pole, laser plasma interakce, Monte Carlo simulace, vysoko dávková radioterapie, VHEE radioterapie, vysoko výkonný laser

Title:

Monte Carlo simulations of radiotherapy treatment with laser accelerated particles

Author: Bc. Vanda Sluková

Abstract: This work focuses on the use of laser-plasma electron accelerators to create very high-energy electrons (VHEE) and other particles for radiotherapy. With use of a general-purpose Monte Carlo code called FLUKA and its graphical interface FLAIR treatment planning of a realistic brain tumor in a simplified geometry and with a realistic treatment device is performed. The geometry of the device is based on the technical design of a laser-driven radiotherapy device designed at ELI-Beamlines. In this work, radiation beams are optimized in terms of

geometry (position around the patient) and treatment time is calculated. Different combination of parameters are considered and time of the treatment is calculated. Treatment planning is also been studied for positron beam. Throughout this work, the pencil beam scanning (PBS) method is used and thus for comparison multi leaf collimator (MLC) approach is explored. Furthermore, the experiment and associated simulation performed at ELI Beamlines by the electron acceleration team are presented as well.

Key words: high dose rate radiotherapy, high power laser, laser wakefield acceleration, laser plasma interaction, Monte Carlo simulation, radiation matter interaction simulation, VHEE radiotherapy

Contents

Introduction

Laser electron accelerators have been proposed by Tajima and Dawson in 1979. The first experimental demonstration of laser wakefield acceleration happened in 2004 by 3 independent groups (USA, UK, France). This new accelerators are very compact and produce electron beams as short as 1 fs, leading to extremely high peak currents. In the light of their advantages, Laser plasma accelerators (LPAs) are being investigated as a potential future source for application in the fields of cancer therapy, ion implantation, electron cutting and welding, and non-destructive testing.

With the evolution of technology, scientists are always trying to find new and better ways of treating cancer. One of the ideas currently investigated is to use very high-energy electrons for radiotherapy with energy between 50-250 MeV. Several studies have been conducted on this topic and very high energy electrons (VHEE) show advantages such as more uniform dose in the target volume, better irradiation of the deep-seated tumors, and higher dose rates can be enabled. Shortcomings connected to the use of VHEE can be overcome.

This thesis focuses on brain cancer radiotherapy treatment planning using VHEE generated from the laser-plasma accelerators. The main goal is to simulate treatment that is effective and fast in realistic configuration and thus answer the question of whether it is beneficial to pursue laser-driven VHEE radiotherapy. To answer this question Monte Carlo simulations have been performed using FLUKA code and Flair graphical interface. The treatment planning has been tested on real patient data anonymized.

In the beginning of this thesis laser-plasma accelerators are introduced and their underlying physics is summarized in Chapter 1. In Chapter 2 the medical motivations of VHEE are presented and convectional technology is described along the new laser plasma technology. Methods of the simulations, properties of the electron beams, description of the machine, and the PTV are outlined in Chapter 3. In Chapter 4 treatment planning for brain cancer is studied and presented in detail. This Chapter includes as well simplified simulation with multi-leaf collimator and positron radiotherapy treatment. In Chapter 5 my experimental work in laser plasma acceleration in high repetition rate is described. Discussion and conclusion are presented at the end of this paper.

Chapter 1

Laser plasma accelerators (LPA)

The first idea to use plasma as an ionized medium for laser electron accelerators was proposed by Tajima and Dawson in 1979 [1]. Since then, many studies and experiments were performed that verified the theory [2, 3, 4, 5]. One of the key advantages of plasma-based accelerators is their ability to sustain an extremely large acceleration gradient. In a typical radio-frequency linear accelerator, the limit of accelerating gradient is $\sim 100 MV/m$. Ionized plasmas can sustain electron plasma waves with electric fields exceeding

$$E_0 = cm_e\omega_p/e \tag{1.1}$$

in typical units is

$$E_0[GV/m] \simeq 96\sqrt{n_0[10^{18}cm^{-3}]}\,, \tag{1.2}$$

where $\omega_p = (4\pi n_0 e^2/m_e)^{1/2}$ is the electron plasma frequency, n_0 is the ambient electron number density, m_e and e are the electron rest mass and charge and c is the speed of light in vacuum. E_0 is called the cold nonrelativistic wave-breaking field [6]. Nowadays electron beams can be accelerated up to 8 GeV in 20 cm plasma [7]. Another unique feature of LPAs is that they can produce extremely short electron bunches as short as fs [8]. In summary, LPA enables generation of high-brightness beams, and kiloampere peak current [9].

1.1 Principles of laser wakefield acceleration

When an intense laser pulse propagates through a plasma, it causes the electrons to move out of its path. The ions in the plasma are much heavier and thus they move in a time scale longer then the duration of an ultra short laser pulse. The forced separation of electrons and ions creates a wake behind the laser pulse (plasma wakefield), which can be used to accelerate charged particles. These plasma oscillations, called plasma waves (in Fig. 1.1), are excited by the ponderomotive force of the laser pulse. The phase velocity of the plasma wave is typically equal to the group velocity of the laser pulse and is less than c. The pattern of wakefield excitation differs significantly for laser pulses longer and shorter than the plasma period. The wakefield will be strongest when the laser pulse duration τ satisfies the condition $\omega_p\tau \approx 1$ [10].

The laser-plasma interaction depends on the laser pulse intensity I and electric field E. The normalized vector potential a_0 is defined as

$$a_0 = 0,855\sqrt{I[10^{18}W/cm^2]\lambda^2[\mu m]}\,, \tag{1.3}$$

where I is the laser intensity and λ is the wavelength of the driving laser [11]. For $a_0 \ll 1$ and $E \ll E_0$, the wakefield generation is in the linear regime. In the linear regime, the plasma wave is a simple sinusoidal oscillation with frequency ω_p and a phase velocity v_p. When $E \gtrapprox E_0$ the plasma wave becomes is nonlinear.

The distance where particles can be accerelated depends on the wavelengths of the plasma wave and the driving laser. The dephasing length for linear regime is

$$L_d \approx {\lambda_p}^3/\lambda^2\,, \tag{1.4}$$

where

$$\lambda_p \approx 2\pi c/\omega_p \tag{1.5}$$

and λ are mentioned wavelength of the plasma and driving laser [11]. The dephasing length express the distance over which electrons are accelerated until they reach a point where they start to decelerate [12].

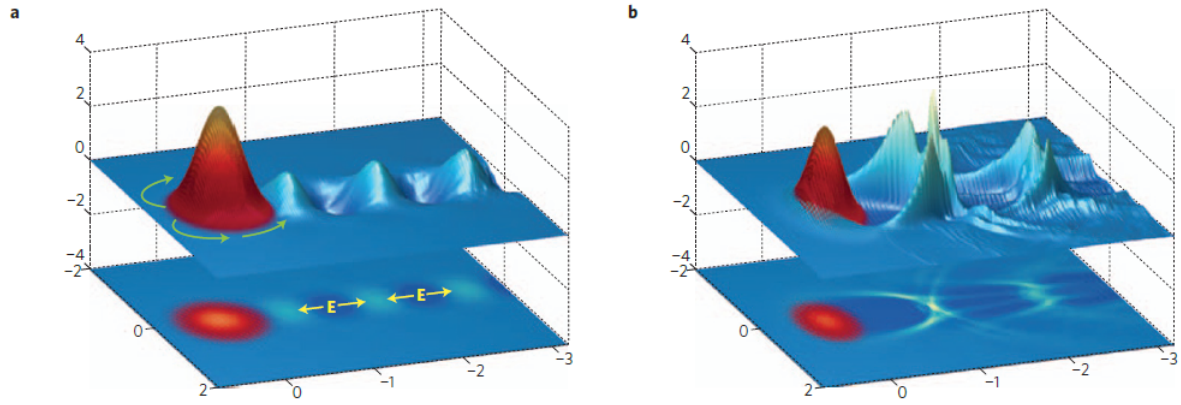

Figure 1.1: Plasma waves driven by intense laser pulses. The laser pulse (red-yellow) propagates from right to left and excites a plasma wave. The normalized intensity laser parameter, a_0, is **a)** a_0= 0.5 corresponding to linear regime and **b)** a_0=4.0 corresponding to nonlinear regime. Image taken from [11].

1.2 Ponderomotive force

The ponderomotive force drives the wakefield and it is the nonlinear time-averaged force experienced by a charged particle as it moves in the field of an electromagnetic pulse. It can be described with electron's ponderomotive energy U_p, which is proportional to laser intensity I. Hence the ponderomotive force is

$$F_p = -\nabla U_p \approx -\nabla I\,. \tag{1.6}$$

To summarize, it pushes the electrons out of the regions of the high gradient in the laser intensity. [11]

1.3 Schemes of LPAs

1.3.1 Plasma beat wave accelerator (PBWA)

Due to the lack of high-energy ultrashort pulse lasers in the early development of LPAs (1979), Tajima and Dawson proposed a new scheme: plasma beat wave accelerator (PBWA). In this scheme, two copropagating laser pulses with frequencies ω_1 and ω_2 are used to excite a relativistic plasma wave (see Fig.1.2 b)). That is achieved only if $\Delta\omega = \omega_1 - \omega_2 = \omega_p$. When this condition is satisfied, large-amplitude plasma waves are generated. When the amplitude of the plasma wave is increasing, the relativistic increase in electron mass reduces the plasma frequency; this shifts the laser beat wave out of resonance and leads to the saturation of the plasma wave amplitude. [11]

1.3.2 Self-modulated laser wakefield accelerator (SMLWFA)

In the early 1990s, the development of high-power lasers was rising. Even though the pulses from chirped pulse amplification (CPA) were too long, they were intense enough to excite a relativistically propagating plasma wave through parametric instability called forward Raman scattering (RFS) [13]. This plasma wave is large enough to trap a lot of electrons and accelerate them in the laser direction, creating an electron beam (see Fig.1.2 c)). This scheme eliminated the need for two laser pulses used in PBWA.

1.3.3 Bubble regime

Nowadays, the bubble regime is used the most, allowing the generation of high-energy quasi monoenergetic electron beams. The quasi monoenergetic electron beam is created when the laser energy is concentrated in a very small sphere. Moreover, the waist w_o of the focused laser pulse becomes matched to the plasma:

$$k_p w_o = 2\sqrt{a_o} \tag{1.7}$$

with

$$k_p = \omega_p / c \tag{1.8}$$

and the pulse duration is of the order of half a plasma wavelength [12]. The radiation pressure (ponderomotive force) expels radially electrons from the plasma leaving a void or a bubble of ions. The void is positively charged behind the laser and is surrounded by a dense region of electrons. Electrons can now be trapped at the back of the cavity and be accelerated by the high electric field (space-charged attraction force of plasma ions). This force attracts the electrons to ions, causing them to overshoot and setting up wakefield oscillations (see Fig. 1.3). The lack of interaction of electrons with the laser, after they are trapped contributes to the improvement of the quality of the beam.

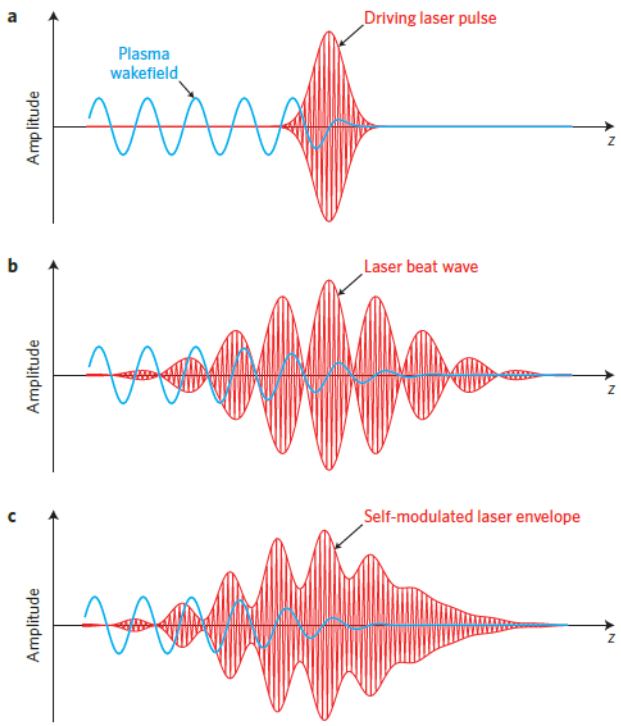

Figure 1.2: Laser-driven plasma acceleration schemes **a)** LWFA **b)** PBWA **c** SMLWFA. Image taken from [11].

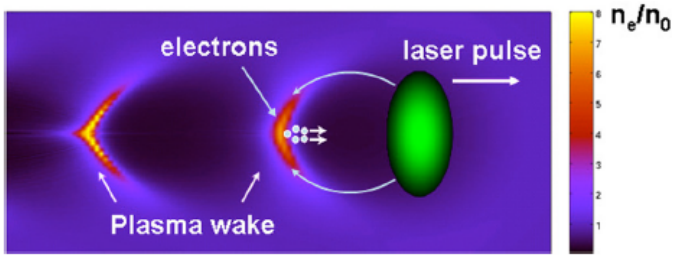

Figure 1.3: The laser pulse that propagating from left to right, expels electrons, creating a positively charged cavity. The radially expelled electrons flow along the cavity boundary and are trapped at the bubble base. After that they are accelerated behind the laser pulse. Image taken from [14].

1.4 Injection of electrons

Controlling the injection and trapping of the electrons is a challenge for LPAs. Electrons have to be injected at the proper phase of the wake or have big enough initial kinetic energy. In case of highly nonlinear plasma wave, the wave breaking can occur leading to trapping electrons in the accelerating field. In the other case, the electrons must pre-accelerated up or the wave slowed down. Several solutions for controlling injection have been proposed, and are described below.

1.4.1 Injection with colliding laser pulses

This scheme relies on the interaction of two intersecting laser pulses (see Fig.1.4). Having two laser beams offers more flexibility and allows to separate the injection from the acceleration process. The pump pulse creates a high amplitude plasma wave and collides at a predetermined location of the plasma wave with a second pulse of lower intensity. The interaction of two laser pulses creates an interference beat pattern with a slow phase velocity, which can be almost zero. That heats some electrons from the plasma background, accelerates electrons in the direction of the plasma wave, and triggers trapping. In this scheme, lower laser intensities can be used, since the ponderomotive beat wave, associated with the interference beat pattern, is much greater than the ponderomotive force associated with the pump laser, which is inversely proportional to the pulse duration at resonance. This scheme has been validated experimentaly [15].

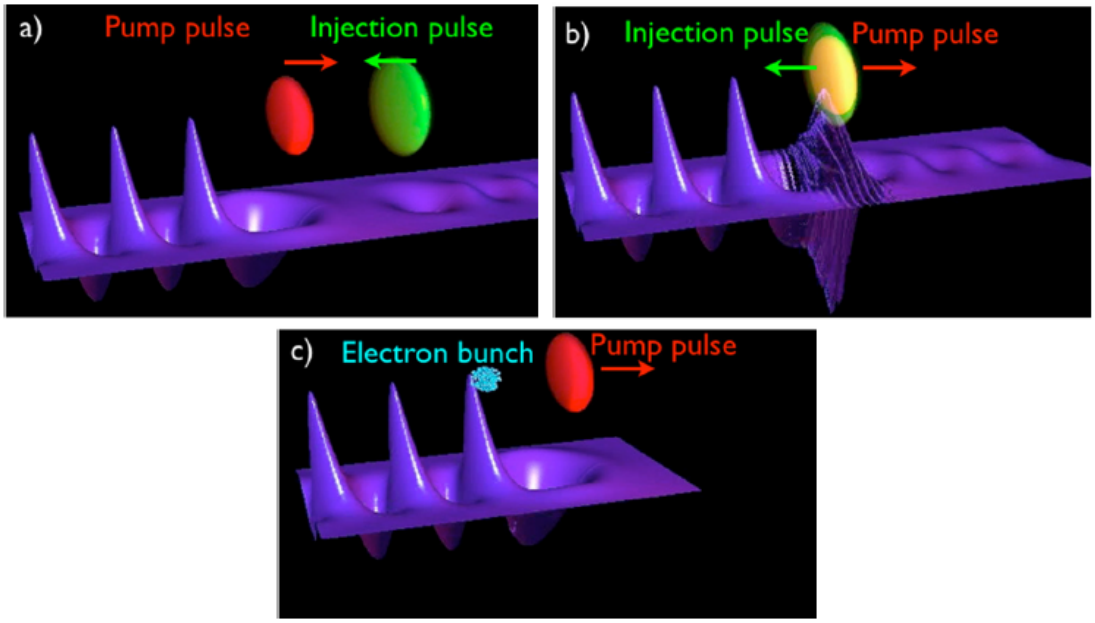

Figure 1.4: Injection with two colliding laser pulses: (a) the two counter-propagating laser pulses, (b) during the collision, some electrons are trapped by the relativistic plasma wave driven by the pump beam, and (c) trapped electrons are then accelerated in the wake of the pump laser pulse. Image taken from [14].

1.4.2 Injection in a density gradient

In this scheme, an approach of slowing down the plasma wave is considered. It was first proposed by Bulanov et al. in 1998 [16]. It involves a downward density ramp, where the density decreases in the direction of the propagated laser. When the laser travels through a decreasing density, the plasma wave velocity slows down. The decrease in the phase velocity allows electrons from the plasma background to be trapped easily. The optimal wake phase velocity for trapping the electrons can be found by adjusting the rate of decrease of plasma density.

1.4.3 Injection triggered by ionization

Injection triggered by ionization using a high-Z gas or high Z low gas mixture is a simple technique for trapping electrons. Because there is a large difference in the ionization potential between consecutive ionization states, only one laser pulse is used to ionize the low energy level electrons of the high-Z gas and after the laser reaches its peak intensity it releases the inner level energy electrons. The inner level energy electrons are thus injected into the front of the wakefield cavity and are accelerated as they move towards the back of the cavity. This injection technique leads to a quite large energy spread of electron beams, caused by the long injection length [17, 18].

In 2015 a new technique was proposed by C. Thaury et al. [19] called shock assisted ionization injection. It proposed to use a shock front[1] transition to localize the injection. This scheme is simpler and leads to a mean energy spread of about 10 MeV. Firstly, the creation of a shock front in the supersonic gas jet occurs. When the laser crosses the shock front, the ionized electrons spend more time in the accelerating field because the cavity expands. Allowing the electrons to be injected below the threshold for a typical ionization injection. This leads to localized trapping and low energy spread.

[1] the advancing edge of a shock wave

Chapter 2

Very high energy electrons (VHEE) in radiotherapy

2.1 Medical motivations of VHEE therapy

After the original work of DesRosiers [20], in the past two decades, several studies and experiments have shown the potential of 100-250 MeV VHEE beams for radiotherapy. In the study by Bazalova-Carter et al. [21] it is demonstrated that 100 MeV VHEE dose distribution for a pediatric brain case and a lung case outperformes the Volumetric Modulated Arc Therapy (VMAT) plans while 100 MeV prostate dose distribution was similar to the clinical VMAT plan. In the last 3 years, FLASH radiotherapy is being investigated in which ultra-high dose rates are used to deliver radiotherapy in a manner that reduces normal tissue toxicity [22, 23].

Very high energy electrons (VHEE) with energies greater than 100 MeV offer several benefits over photons and protons currently used in radiotherapy treatment. A small diameter high-energy electron beam can be scanned and focused easily. The rapid electromagnetic scanning can make the use of multileaf collimators and other mechanical parts unnecessary. VHEE beams are as well suitable for the treatment of deep-seated tumors, due to their high inertia and small penumbra. Furthermore, VHEE beams have the ability to preserve electronic equilibrium at the boundaries between different density tissues. This leads to a more uniform dose in the target volume. These properties contribute to the improvement of the ratio of target dose to dose to healthy tissue. Moreover, several studies have shown that VHEE beams can achieve a very good dose conformation, in comparison with the photon treatment [20, 24, 25]. Other advantages of VHEE beams include their possibility to irradiate the target from several different directions at the same time, their femtosecond to picosecond duration electron bunches, which leads to a very high dose rate, and energies that exceed the ones currently used in clinical applications.

VHEE radiotherapy treatment is faster than photon plans, because of these three effects:

- The efficiency of production of the X-ray beams from linear accelerators is smaller than for VHEE
- Fewer electrons are needed to deliver the same dose as photons
- The electron beams can be steered electromagnetically in the order of milliseconds

The problem with VHEE arises when only one beam is used. The depth dose distribution of a single, collimated VHEE beam is quasi-uniform, which can lead to healthy tissue being overexposed. This issue can be overcome with the use of several beams and focusing the VHEE beam to a small spot. [26, 27]

2.2 VHEE with radio frequency (RF) technology

A medical linear accelerator (LINAC) is the device most commonly used for external beam radiation treatment for patients with cancer. LINACs contain RF cavities, an electromagnetic field situated in the metallic chambers, where the acceleration takes place. The field in an RF cavity oscillates at a given frequency, therefore to accelerate the particles, injection of the particle to the RF cavity is crucial. Klystron, the tube containing electron beams, is used to drive the cavities. The energy of the beam is delivered to the cavity through the metal waveguide. Charged particles that are injected into to RF cavity receive an electrical impulse that accelerates them.

Several studies and experiments have been conducted in the last decades that focused on the use of LINACs VHEE beams for radiotherapy. For example, dose measurements were performed by A. Subiel et al in 2014 [25] (see Fig. 2.1). Few years later the study of the temporal and spectral evolution of ultrashort VHEE beams in a water phantom and ion recombination measurements have been conducted by A. Subiel et al in 2017 [28] as well. The development and the use of pluridirectional high-energy agile scanning electronic radiotherapy (PHASER) for ultra-rapid highly conformal image-guided radiation has been studied by P.G. Maxim et al. in 2019 [23]. The research of PHASER is based on the technology of RF linear accelerators. Importantly, the PHASER technology has the potential of getting superior FLASH radiobiological therapeutic index and eliminating the impact of tumor motion.

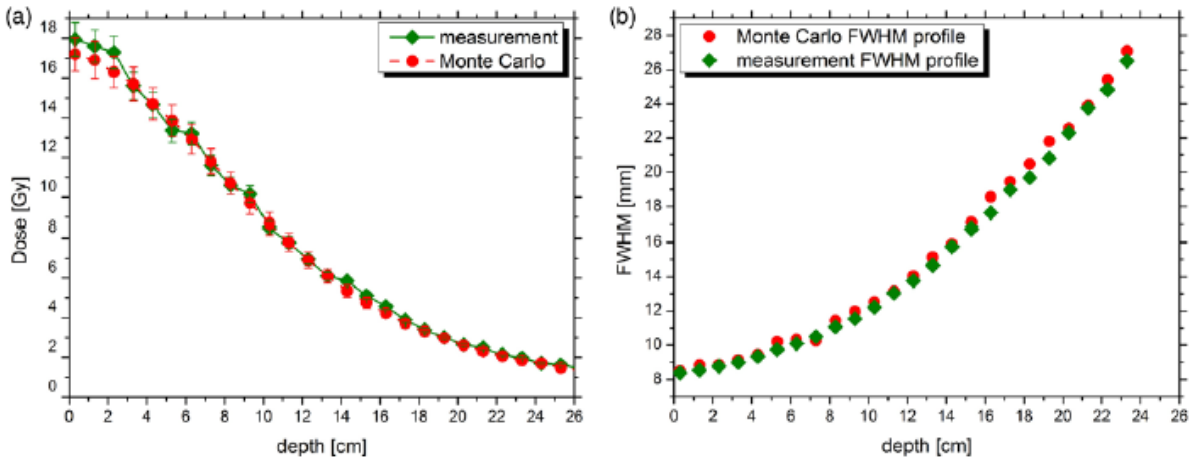

Figure 2.1: (a) Depth dose profile for 165 MeV electron beam from the convectional linear accelerator. (b) Evolution of the FWHM beam profile as a function of depth within the water phantom. Image taken from [25].

Among the advantages of VHEE radiotherapy, some downsides to this treatment arise as well. For example, as a consequence of working with only one collimated VHEE beam, healthy tissue can become overexposed. Overcoming this problem is done in two ways: a) using more beams or b) focusing of the beams to achieve the concentration of dose into a small volume. Option b) has been examined in 2021 by K. Kokurewicz et al ([26]). The measurement of the depth-dose profile of 158 and 201 MeV VHEE beams in the water phantom has been completed. Altogether, they came to a conclusion that focused VHEE beams concentrate dose into a well-defined volume deep in the tissue, while the dose delivered to the surrounding tissue is scattered over a large area, thus reducing entrance and exit dose. Furthermore focusing on the beam is useful in FLASH radiotherapy, where therapeutic doses are delivered at high rates. Additionally, symmetric and asymmetric focusing of the beams using quadrupoles have been studied and described by L.Whitmore et al in 2021 ([22]). They arrived to the same conclusion, such as the improvement of the entrance dose is achieved when focusing of the beam is implemented (see Fig.2.2). Increasing the beam energy from 100 to 250 MeV decreased the entrance dose by a further 20%, from 45 to 25%. [22]

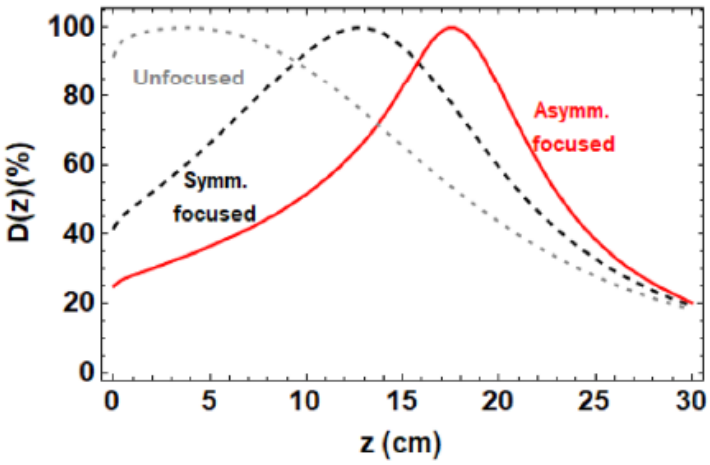

Figure 2.2: Monte Carlo simulations of the normalised on-axis dose plots for 250 MeV symmetric and asymmetric focused beams, as well as unfocused 250 MeV VHEE. Image taken from [22].

2.3 VHEE with laser-plasma accelerators

LPAs were examined thoroughly in Chapter 1, in addition, the focus in this section is on the VHEE from laser-plasma accelerators.

In 2008, the Monte Carlo simulations of dose distributions on a human prostate using the parameters from the LPA were conducted by C. DesRosiers et al [24]. In short, the resulting dose distributions of VHEE were comparable to photon beam distribution. Approximately a year later a similar simulation was executed by T. Fuchs et al [29]. Simulations focus on the influence of the beam characteristic on the dose distribution. From the dose volume histograms (DVH) it appears that for the clinical treatment volume (CTV) and planning target volume (PTV) better dose uniformity in the target volumes is accomplished. In comparison with the conventional photon plan, gross tumor volume (GTV) dose coverage is comparable. Besides, better coverage of the targeted volume sparing of the bladder and rectum is obtained and tumor to normal tissue dose ratio is greater using VHEE from LPA.

Following in 2014, dosimetric measurements for 135 MeV electrons were presented in the paper by A. Subiel et al [25]. Measurements were performed with EBT2 Gafchromic film as well as for 165 MeV from convectional linear accelerator (see Sec. 2.2 Fig. 2.1). The results for VHEE from LPA can be seen in Fig. 2.3 and 2.4. Due to different beam parameters from the linear accelerator and LPA, the dose depth profiles of VHEE are distinct. Moreover, this study arrives at a conclusion that neutron and proton production due to irradiation of VHEEs does not significantly affect the equivalent doses.

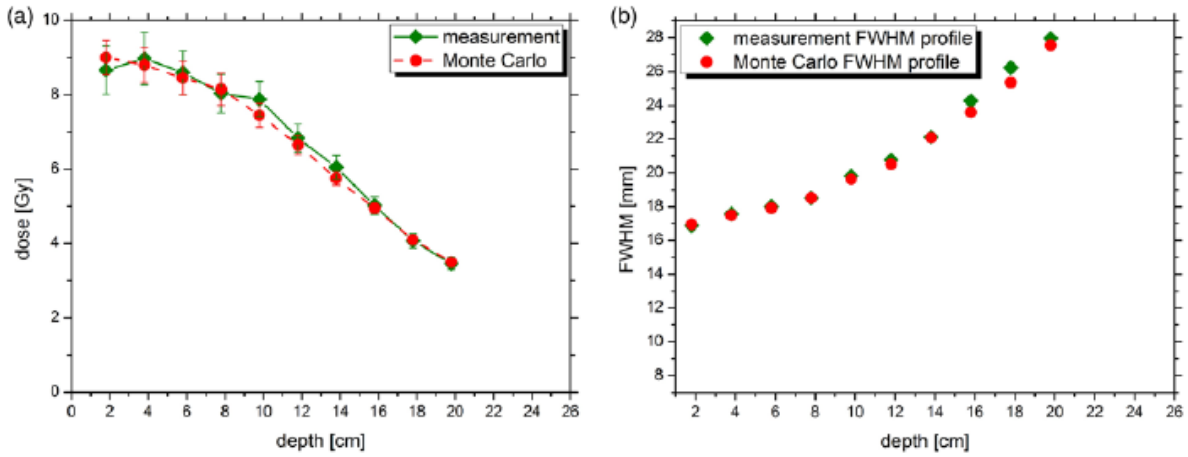

Figure 2.3: Depth dose profile for 135 ± 44 MeV (rms) LPA electron beam (b) Evolution of the FWHM beam profile as a function of depth within water phantom. Image taken from [25].

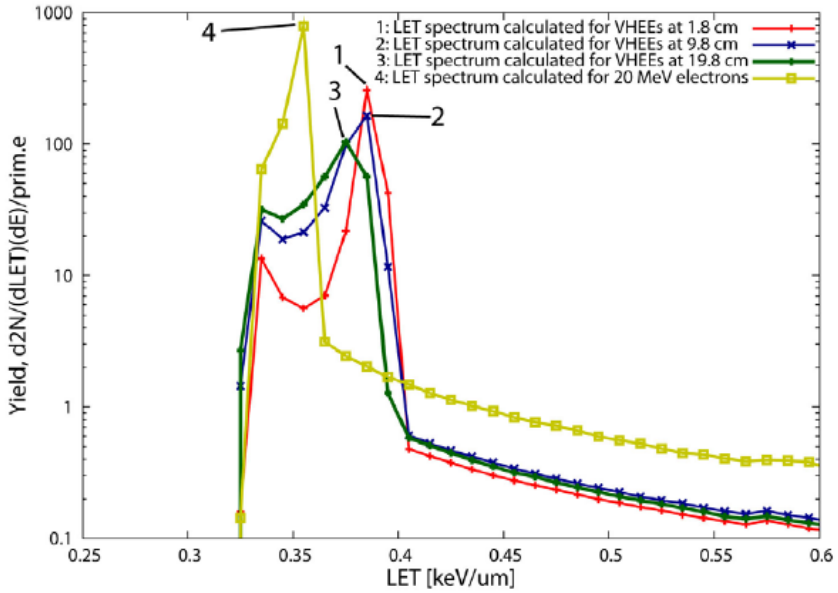

Figure 2.4: Linear energy transfer (LET) spectra calculated for 135 MeV electron beams at EBT2 films positioned at 1.8, 9.8 and 19.8 cm in the water bath. Furthermore the calculated 20 MeV electron LET spectrum is included. Image taken from [25].

Chapter 3

Methods

3.1 Monte Carlo simulation of radiation matter interaction with FLUKA code

Monte Carlo (MC) simulations are an essential tool for the design and commissioning of novel clinical facilities, allowing a detailed description of the beamline and the delivery system. MC techniques can be more effective compared to traditional analytical methods in the following aspects. MC methods work with a more realistic composition of the human body, with a possible advantage over the water-equivalent approach typically used in analytical TPS's. MC methods naturally include mixed field description and three-dimensional spread of the particle fluence, reliably describing the transport, and the interaction of the primary beam and the secondaries. [30]

3.1.1 About FLUKA and Flair

The FLUKA code is a general-purpose Monte Carlo code simulating the interaction and transport of hadrons, heavy ions, and electromagnetic particles from few keV (or thermal energies for neutrons) to Cosmic Ray energies in arbitrary materials. FLUKA has a wide range of applications, spanning accelerator design and shielding, radiation protection, particle physics, dosimetry, detector simulation, hadron therapy. Also, FLUKA is one of the first general-purpose MC codes, which translates DICOM files into voxel geometry as part of the combinatorial geometry package of FLUKA.

Recent developments in the user interface Flair enables working in FLUKA to an increasing number of users. Flair is an advanced user-friendly interface for FLUKA to simplify the editing of FLUKA input files, execution of the code, and visualization of the output files. It is based entirely on python and Tkinter. Among some of the features of Flair belongs: input editor, interactive geometry editor, advanced layer mechanism for graphically displaying any information from the input file on top of the geometry. [31]

3.2 Phantom

The simulations were performed on an anonymized CT scan of a patient diagnosed with Glioblastoma using FLUKA Monte Carlo code. The regions of interest (PTV, brain stem, right eye, and left eye) were contoured by medical staff. Glioblastoma is located in the upper area of the skull (see Fig. 3.1).

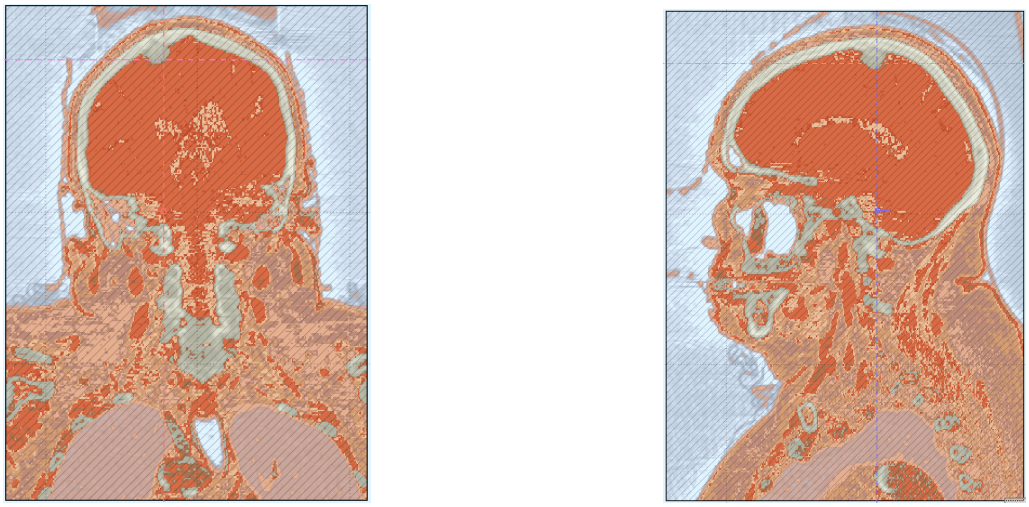

Figure 3.1: The tumor location within the patient´s skull.

3.3 PTV volume

The PTV is a geometric concept created to ensure that the radiotherapy prescribed dose is actually delivered to the CTV. It is a volume related to the isocentre of the linear accelerator rather than to the anatomy of the patient. Volume of the PTV was estimated to be around $V \approx 8\,\mathrm{cm}^3$ with radius $R_{PTV} = 1,3$ cm as can be seen from Fig. 3.2.

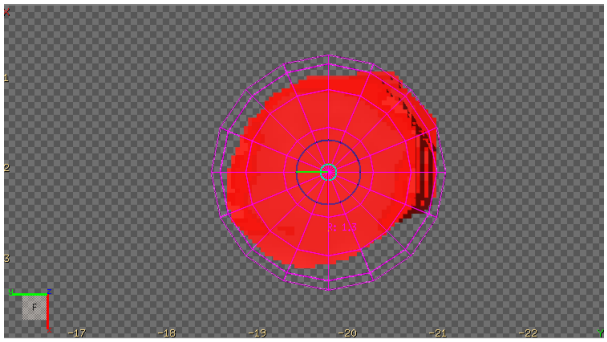

(a) PTV volume from YX plane.

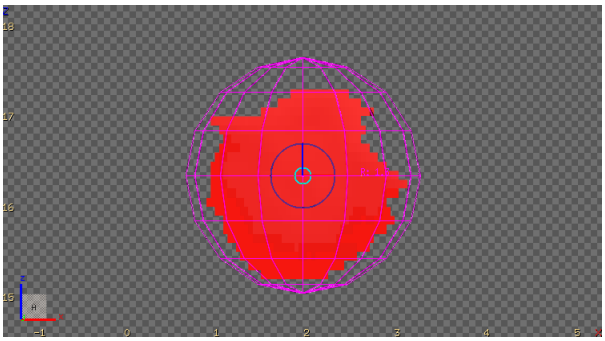

(b) PTV volume from ZX plane.

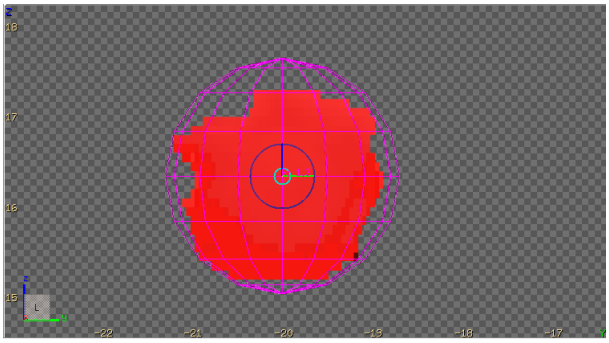

(c) PTV volume from ZY plane.

Figure 3.2: PTV volume approximated with a sphere.

3.4 Radiation beams

The electron beam input parameters (beam shape, FWHM, divergence, momentum spread, and electron energy) are based on recent experimental results [9, 19]. Beam parameter values are summarized in Table 3.1. For better understanding beam parameters are illustrated on Fig. 3.3 and 3.4 . Beam diameter is measured at the value $1/e^2$ of the gaussian curve. In gaussian-shaped beams, the value of beam diameter is d $\approx 1.7 * FWHM$. A total of 7 electron beams were used. Throughout this work, the positioning of the phantom was changed to optimize the cancer treatment plan. To lower the dose in the OARs (organs at risk) to a minimum, the phantom was positioned in a way to reduce the travel distance through healthy tissue before and after the tumor (laid on the side), and thus not intersect with the OARs. The device geometry can be seen in Fig. 3.5. Beams were initialized in a vacuum inside of the machine on a circular orbit 60 cm from the phantom. The beams were coplanar and their positioning is shown in Fig. 3.6.

Beam shape	Gaussian
Electron energy	120 MeV
Momentum spread type	Gaussian
Momentum spread FWHM	0.23 GeV/c
FWHM	0.05 cm
Divergence	1 mrad
Beam diameter	0.085 cm

Table 3.1: Electron beam parameters.

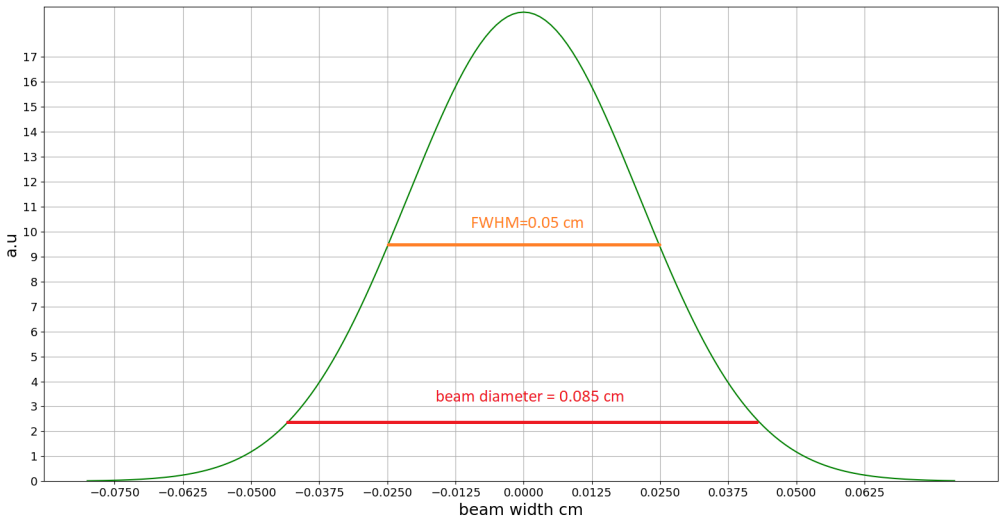

Figure 3.3: Beam shape with corresponding parameters.

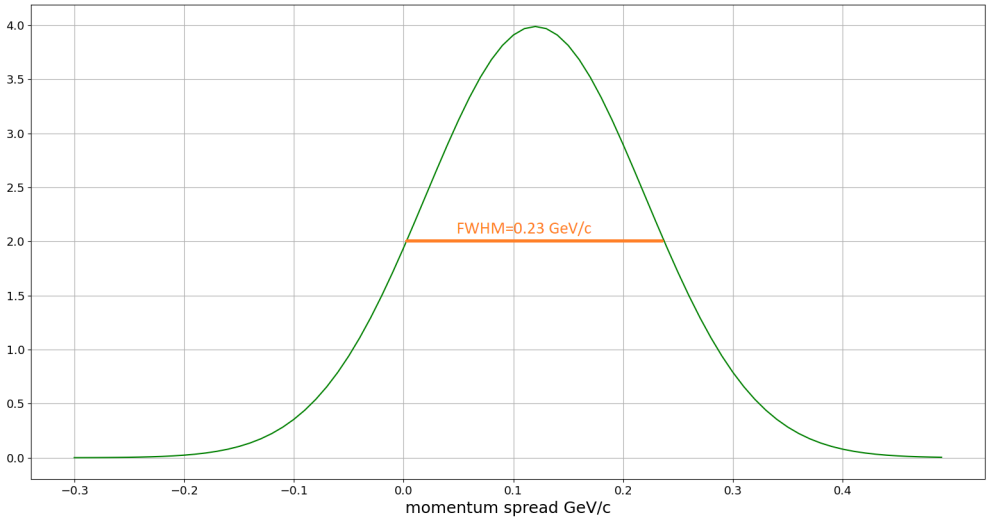

Figure 3.4: Momentum spread with corresponding parameters.

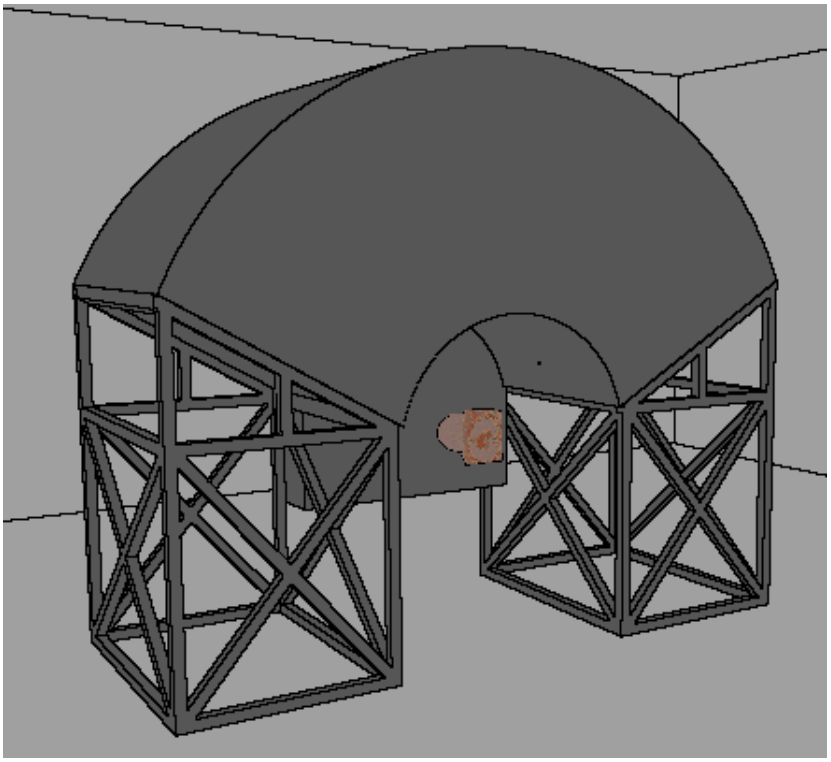

Figure 3.5: Device geometry built in FLUKA.

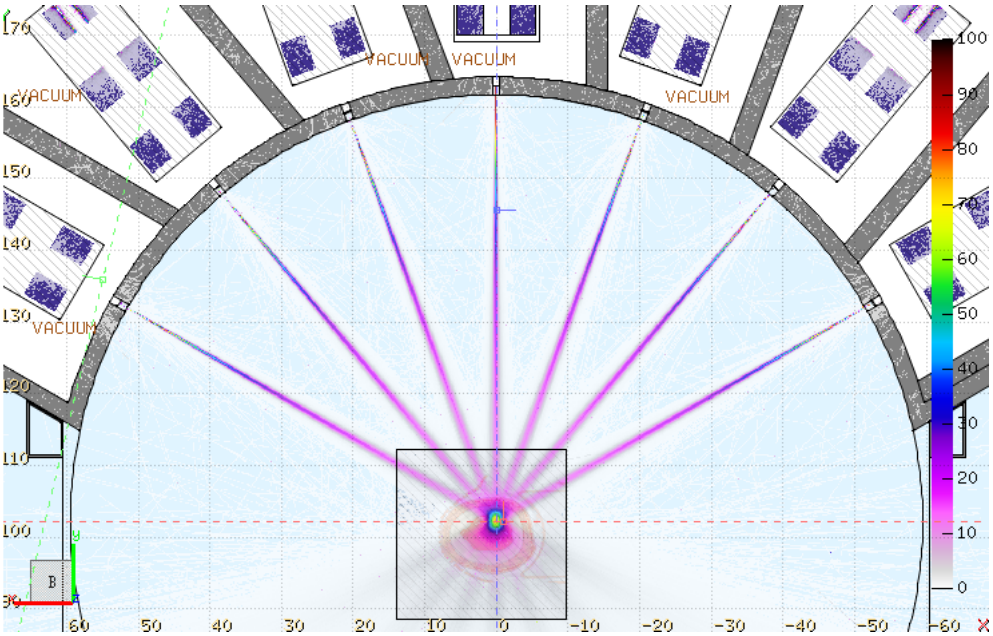

Figure 3.6: Electron beam position in the machine.

Chapter 4

Treatment planning

4.1 Positioning of the phantom versus the time of the treatment

As it was discussed in Chapter 3, since the position of the Glioblastoma is in the upper left side of the skull, the patient (phantom) was laid on the side for better sparing of the surrounding tissue. From the beam parameters, it is clear that the beam is quite narrow and the PTV volume is quite large in comparison to the beam. Thus the need for changing the position of the patient arises. For proper irradiation of the tumor, moving the patient is necessary. Nevertheless, the time of the treatment must be considered as well. Hence compromise must be found to achieve fast and quality treatment. As it was mentioned in Chapter 2, electrons are able to deliver the same dose as protons in a much faster way. That fact significantly lowers the time of the treatment.

The simulations were run for 100 different positionings of the phantom. The dose deposition for 10, 50 and 100 positions can be seen on Fig. 4.1, 4.2 and 4.3. The DVH plot for 10, 50 and 100 positions can be seen on Fig. 4.6, 4.7 and 4.8.

Each simulation (= 1 position) was run with 2 cycles and with 30 000 primaries per cycle. For the calculation of treatment time, the average dose delivered to the PTV had to be calculated. For this calculation, the dose volume histogram has been used (Fig. 4.4). FLUKA gives values in GeV/g, to get dose rate in Gy/s the following formula needs to be used

$$R[Gy/s] = \alpha \cdot I \cdot D_{avg}[GeV/g] \,, \tag{4.1}$$

where α is the multiplying constant, I is beam current and D_{avg} is the average absorbed dose in the PTV. The multiplying constant α is derived as:

$$Gy = \frac{J}{kg} \tag{4.2}$$

$$Gy = \frac{J}{1000g} \tag{4.3}$$

$$Gy = \frac{6.24150907 \cdot 10^{18} eV}{1000g} \tag{4.4}$$

$$Gy = \frac{6.24150907 \cdot 10^{15} eV}{g} \tag{4.5}$$

$$1.602176462 \cdot 10^{-16} Gy = \frac{eV}{g} \tag{4.6}$$

$$1.602176462 \cdot 10^{-7} Gy = \frac{GeV}{g} \, . \tag{4.7}$$

I is calculated as

$$I = Q \cdot f \cdot N_{beams} \, , \tag{4.8}$$

where Q is number of electrons per shot, N_{beam} is number of beams and f is the repetition rate. Next, the time needed to deliver the desired dose has to be calculated.

$$t_{dose} = \frac{D_{desired}}{R} \, , \tag{4.9}$$

where $D_{desired}$ is desired dose. Additionally, the time for changing the position of the patient must be accounted for as well. Since it is just a small distance, 1 second per change of position is expected. In conclusion, for 10 positions an additional 10 seconds have to be added to the treatment time. Calculated times of treatments are shown in Table 4.1 and times for different combinations of parameters are shown in Table 4.2. The most realistic configuration is highlighted.

Number of positions	Time [s]
10	38
50	84
100	136

Table 4.1: Calculated times of radiotherapy treatment for different number of positions.

D_desired[Gy]	Q[pC]	f[Hz]	N	t_dose[s]
1	10	1000	7	2.82
1	10	1000	5	3.94
1	10	1000	1	$1.97 \cdot 10$
1	1	1000	7	$2.82 \cdot 10$
10	**10**	**1000**	**7**	**$2.82 \cdot 10$**
1	1	1000	5	$3.94 \cdot 10$
10	10	1000	5	$3.94 \cdot 10$
1	1	1000	1	$1.97 \cdot 10^2$
10	10	1000	1	$1.97 \cdot 10^2$
10	1	1000	7	$2.82 \cdot 10^2$
1	10	10	7	$2.82 \cdot 10^2$
100	10	1000	7	$2.82 \cdot 10^2$
10	1	1000	5	$3.94 \cdot 10^2$
1	10	10	5	$3.94 \cdot 10^2$
100	10	1000	5	$3.94 \cdot 10^2$
10	1	1000	1	$1.97 \cdot 10^3$
1	10	10	1	$1.97 \cdot 10^3$
100	10	1000	1	$1.97 \cdot 10^3$
1	1	10	7	$2.82 \cdot 10^3$
100	1	1000	7	$2.82 \cdot 10^3$
10	10	10	7	$2.82 \cdot 10^3$
1	1	10	5	$3.94 \cdot 10^3$
100	1	1000	5	$3.940 \cdot 10^3$
10	10	10	5	$3.94 \cdot 10^3$
1	1	10	1	$1.97 \cdot 10^4$
100	1	1000	1	$1.97 \cdot 10^4$
10	10	10	1	$1.97 \cdot 10^4$
10	1	10	7	$2.82 \cdot 10^4$
100	10	10	7	$2.82 \cdot 10^4$
10	1	10	5	$3.94 \cdot 10^4$
100	10	10	5	$3.94 \cdot 10^4$
10	1	10	1	$1.97 \cdot 10^5$
100	10	10	1	$1.97 \cdot 10^5$
100	1	10	7	$2.82 \cdot 10^5$
100	1	10	5	$3.94 \cdot 10^5$
100	1	10	1	$1.94 \cdot 10^6$

Table 4.2: Calculated times of radiotherapy treatment for $D_{avg} = 5.072052677 \cdot 10^{-6}$ GeV/g, electron energy E_{beam}=120 MeV, momentum spread p=0.23 GeV/c and 1 position.

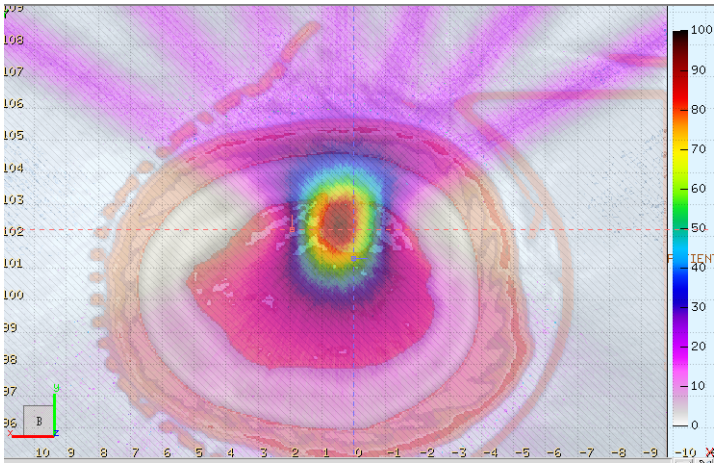

(a) 2D plot of dose deposit in the phantom from XY plane.

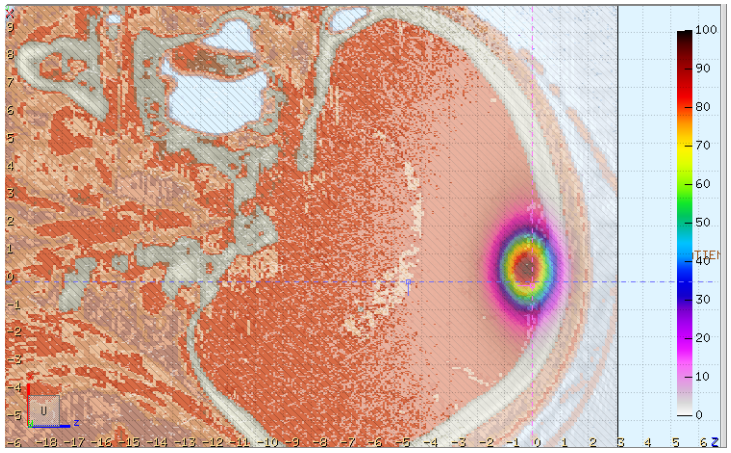

(b) 2D plot of dose deposit in the phantom from ZX plane.

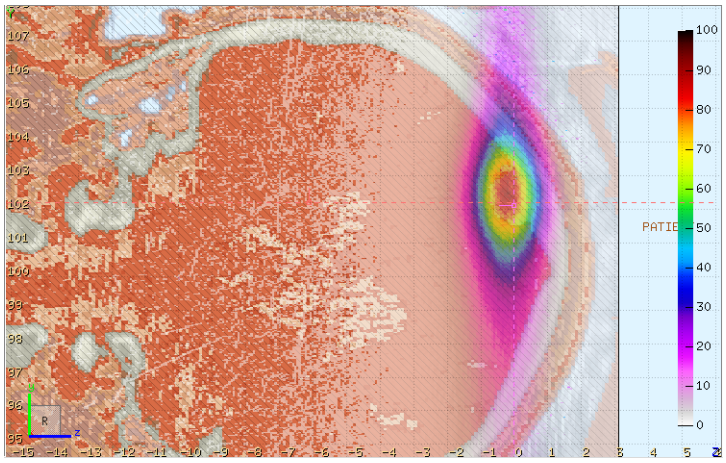

(c) 2D plot of dose deposit in the phantom from ZY plane.

Figure 4.1: Dose deposition for 10 positions.

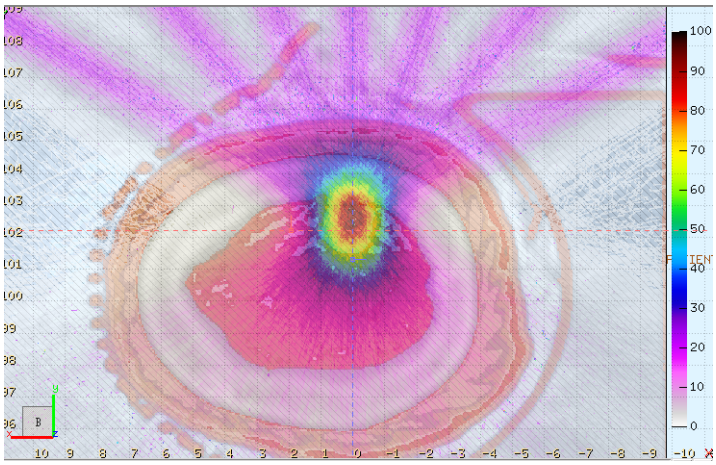

(a) 2D plot of dose deposit in the phantom from XY plane.

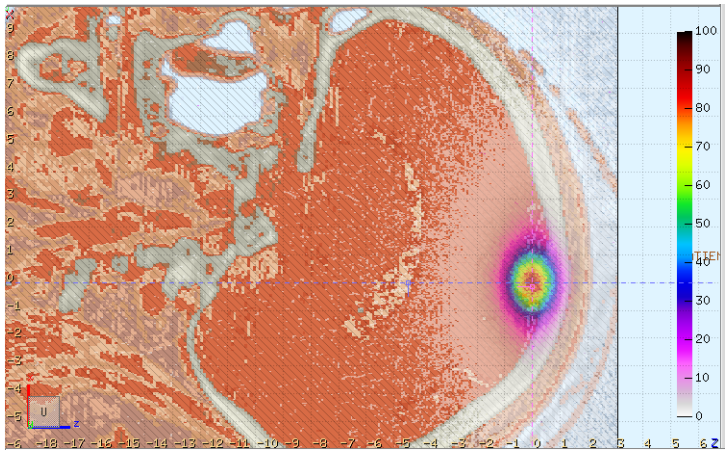

(b) 2D plot of dose deposit in the phantom from ZX plane.

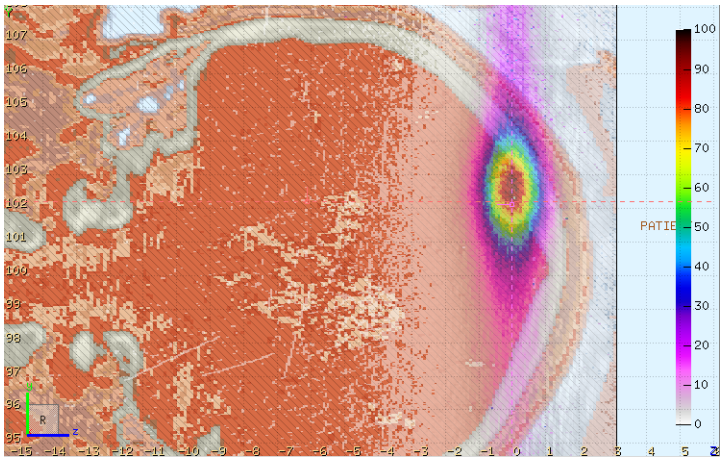

(c) 2D plot of dose deposit in the phantom from ZY plane.

Figure 4.2: Dose deposition for 50 positions.

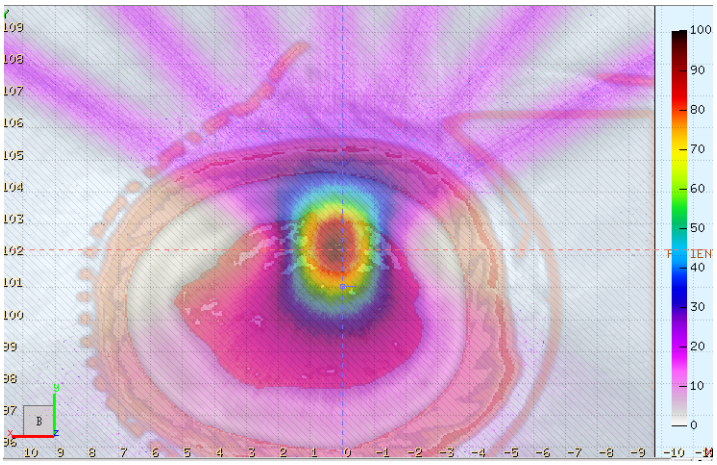

(a) 2D plot of dose deposit in the phantom from XY plane.

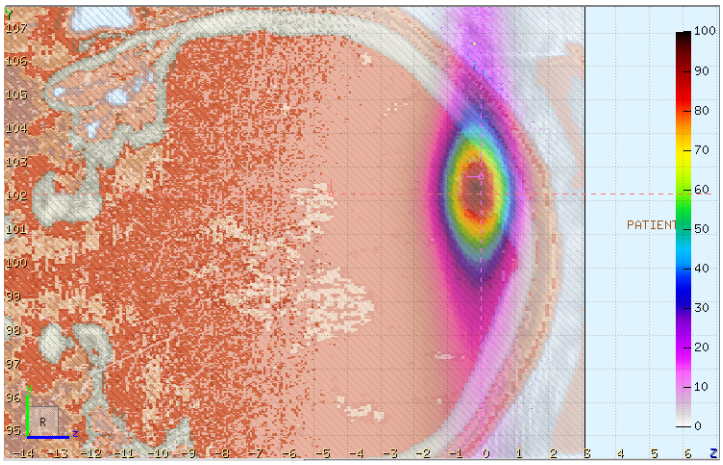

(b) 2D plot of dose deposit in the phantom from ZX plane.

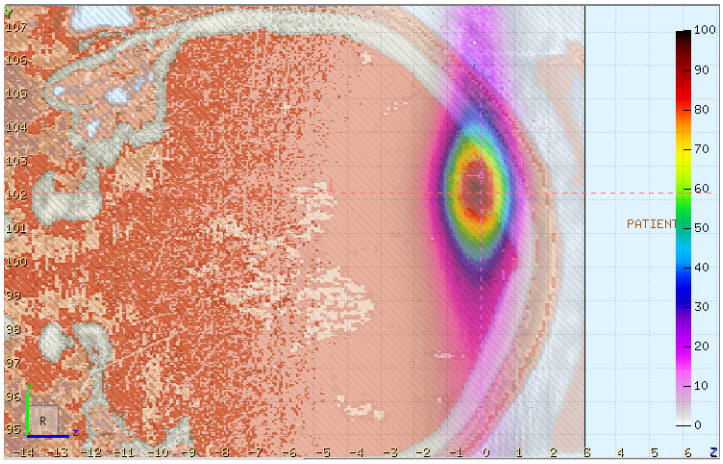

(c) 2D plot of dose deposit in the phantom from ZY plane.

Figure 4.3: Dose deposition for 100 positions.

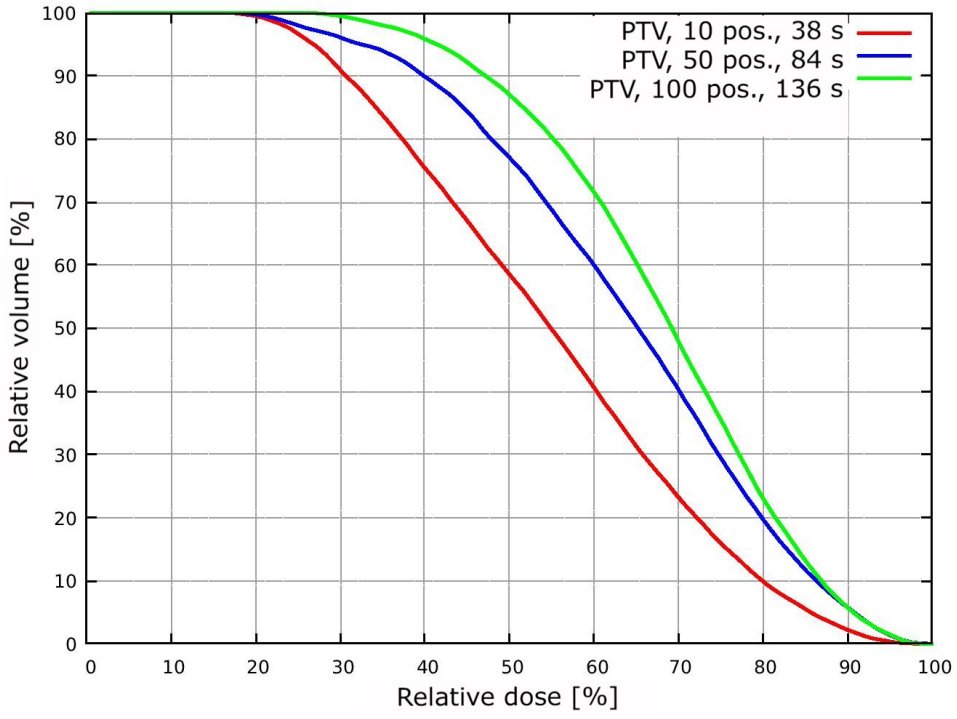

Figure 4.4: DVH plot and time comparison of positions of the patients.

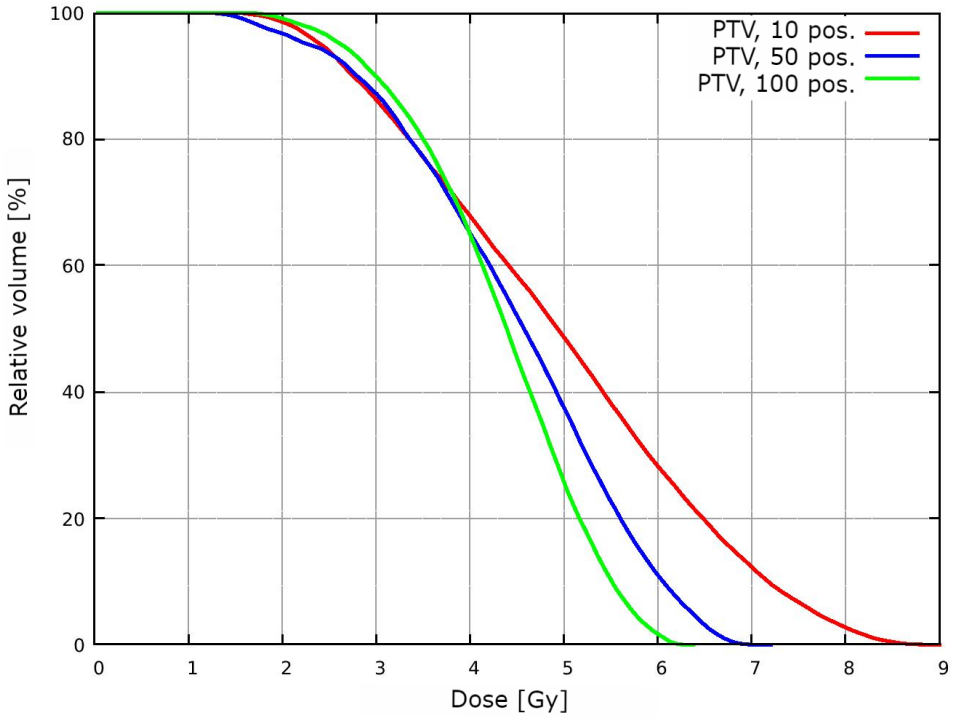

Figure 4.5: DVH plot showing distribution of dose [Gy] in PTV for 1 second.

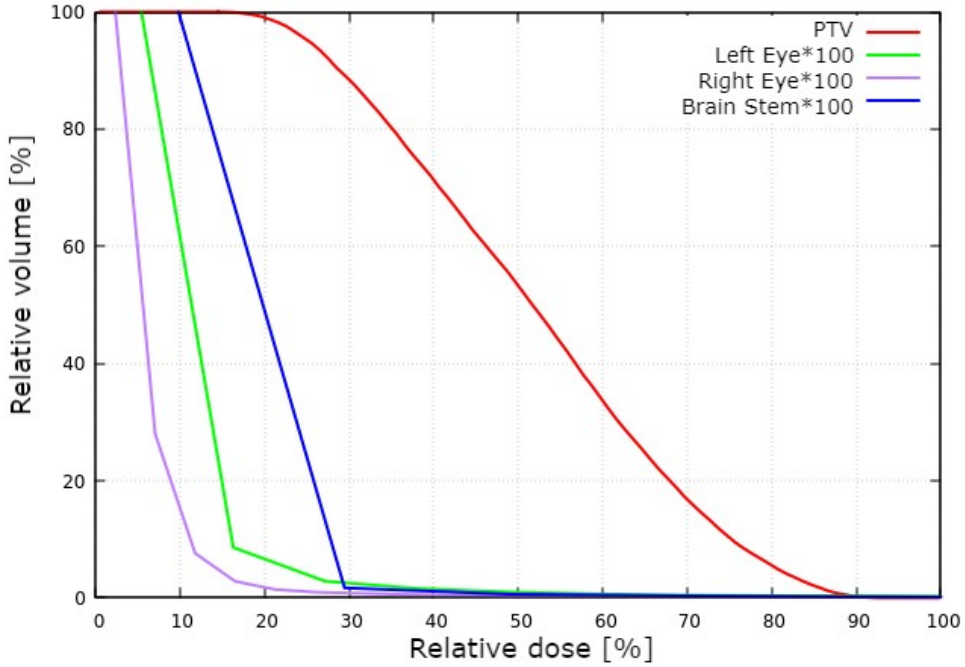

Figure 4.6: Normalized DVH plot showing organs at risk (OARs) and PTV for 10 positions.

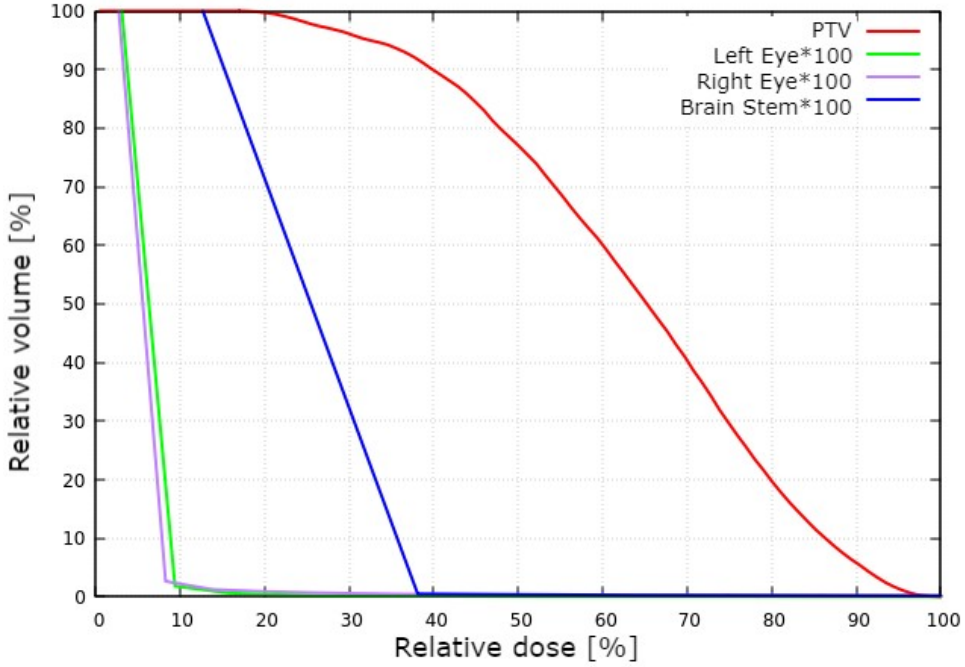

Figure 4.7: Normalized DVH plot showing organs at risk (OARs) and PTV for 50 positions.

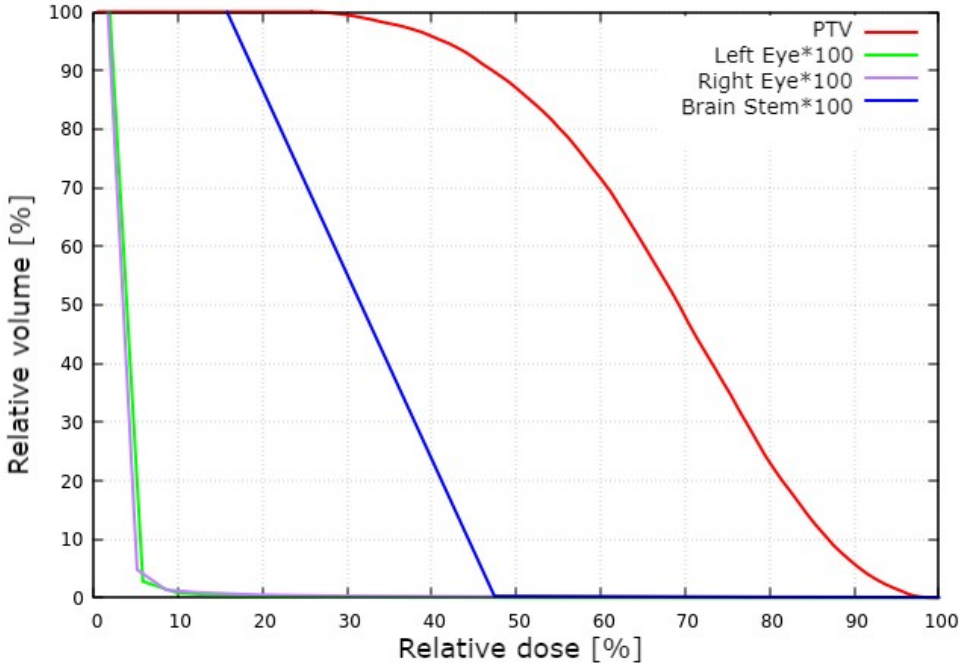

Figure 4.8: Normalized DVH plot showing organs at risk (OARs) and PTV for 100 positions.

4.2 Positron treatment planning

The utilization of positrons for radiotherapy is currently being investigated [32]. For this reason, the study of VHEE beams for radiotherapy has been extended also for the case of positron beams with comparable energy.

Positron beams with energy 100-300 MeV can be generated by sending an electron beam into a high Z target. Using laser-accelerated electron beams can produce a positron beam with 100-300 MeV energy, as shown in experiments [33]. With 0.1-0.3 PW laser systems, 0.2-0.3 nC, 0.3-0.6 GeV electron beams can be produced [33], [34]. Beams with such parameters have the optimal energy for the production of 100-300 MeV positron beams.

The total positron yield is about 0.5 positrons per primary electron, however, most positrons have kinetic energy below 200 MeV. Majority of the positrons are produced by low energy (1 – 100 MeV) gamma photons. Positron yield at 300 MeV is about 0.02 per primary electron at this electron beam energy. An increase of electron beam energy slightly shifts the mean energy of positrons and broad energy distribution, thus the momentum spread has been changed for bigger energies. Simulations were run with 30 000 primaries with 2 cycles. Positron beam parameters are included in Table 4.3.

Dose deposition in the phantom can be seen on Fig. 4.10 for 100 MeV and on Fig. 4.11 for 200 MeV. Comparison of the dose volume is plotted on Fig. 4.9.

Positron energy	200 MeV	100 MeV
FWHM	0.03 cm	0.03 cm
Divergence	30 mrad	30 mrad
Momentum spread FWHM	0.1 GeV/c	0.0 5GeV/c

Table 4.3: Positron beam parameters.

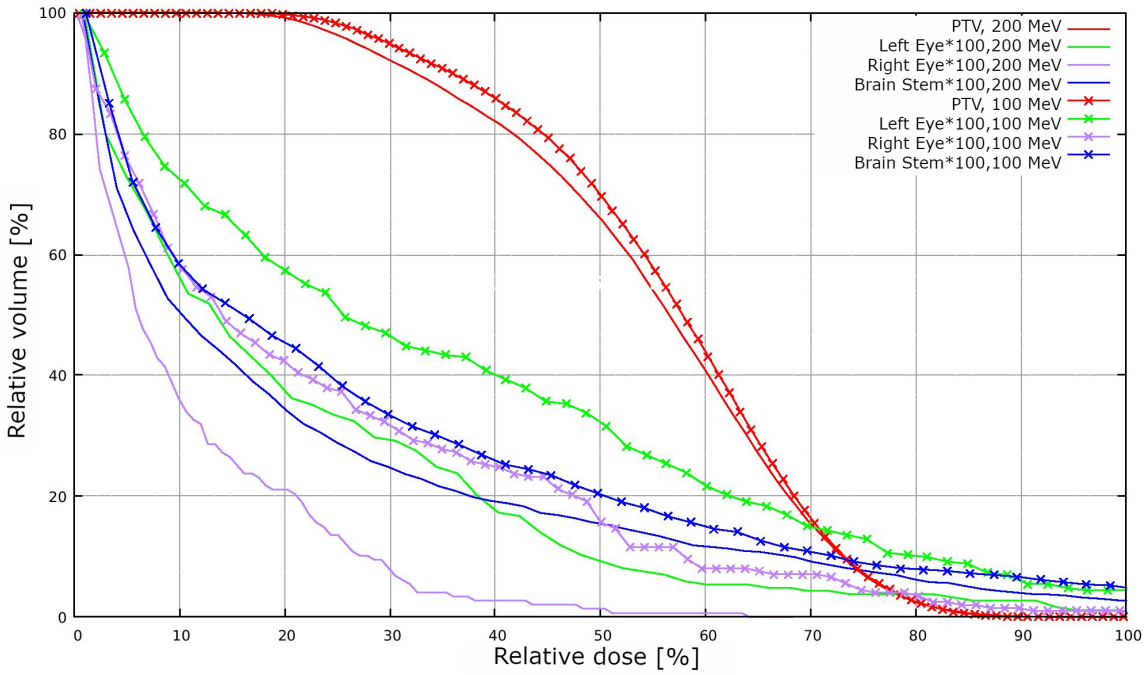

Figure 4.9: DVH plot comparing 2 positron simulations (200 MeV with momentum spread 0.05 GeV/c vs 100 MeV with momentum spread 0.1 GeV/c).

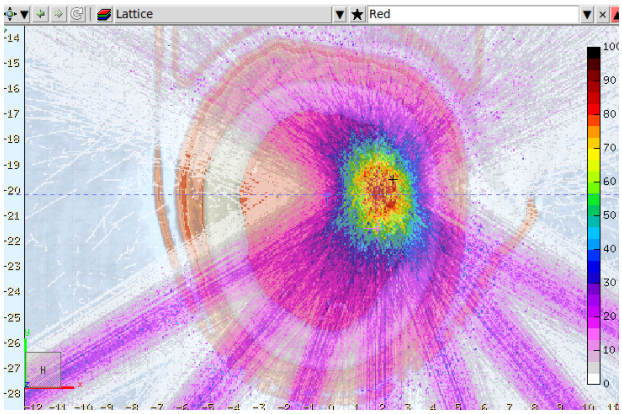

(a) 2D plot of dose deposit in the phantom from XY plane.

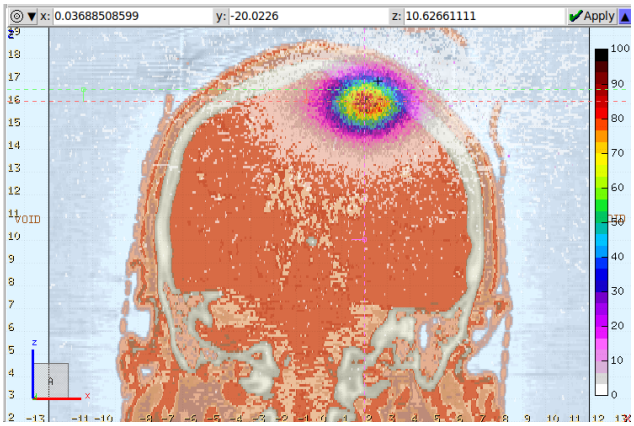

(b) 2D plot of dose deposit in the phantom from ZX plane.

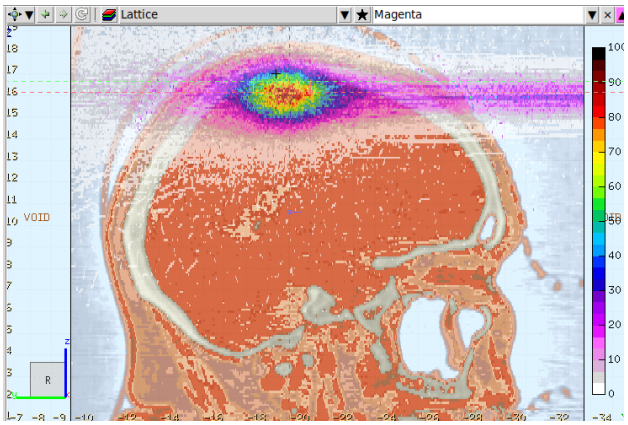

(c) 2D plot of dose deposit in the phantom from ZY plane and FWHM 0.5mm.

Figure 4.10: Dose deposition of 100 MeV energy positrons with 30 mrad divergence, FWHM of 0.03 cm and 0.1 GeV/c momentum spread FWHM

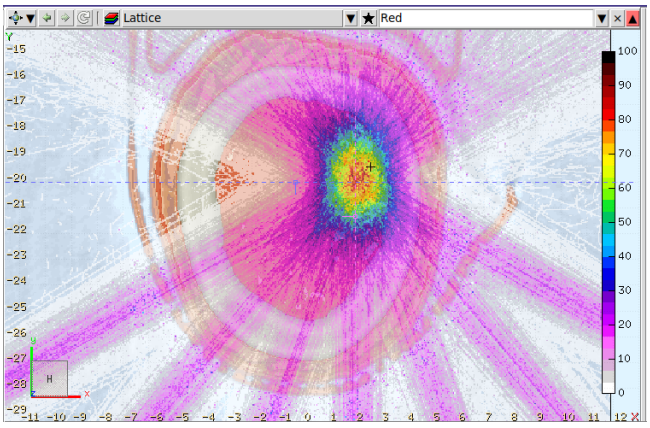

(a) 2D plot of dose deposit in the phantom from XY plane.

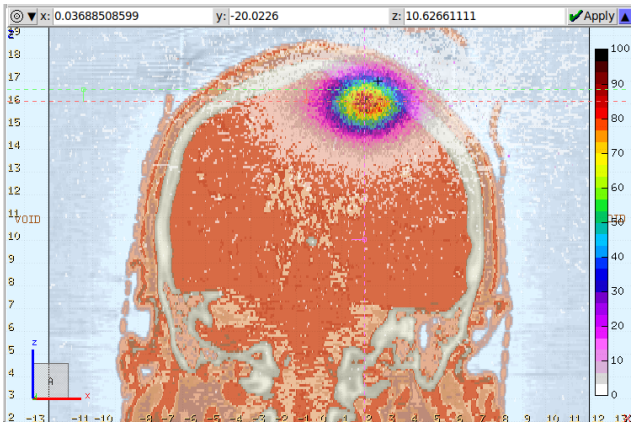

(b) 2D plot of dose deposit in the phantom from ZX plane.

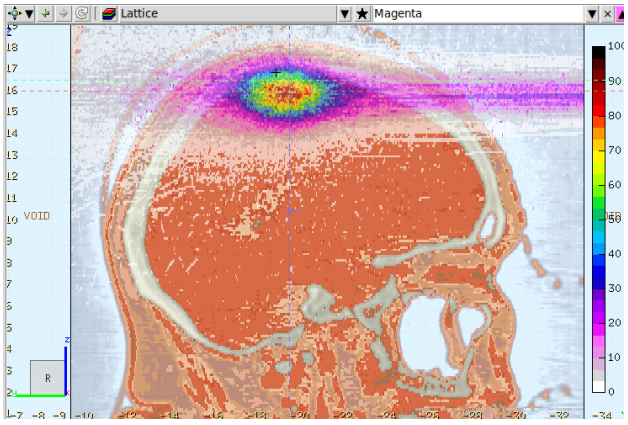

(c) 2D plot of dose deposit in the phantom from ZY plane and FWHM 0.5mm.

Figure 4.11: Dose deposition of 200 MeV energy positrons with 30 mrad divergence, FWHM of 0.03 cm and 0.05 GeV/c momentum spread FWHM

4.3 Multileaf collimator simplified

One of the main goals in radiotherapy is to minimize the dose deposited in healthy tissue and OARs surrounding the PTV. In the case of radiotherapy treatment with large beams, multileaf collimators (MLC) are used to shape the beam into the desired shape. The MLC usually consists of 40 to 120 movable leaves arranged in pairs. This construction allows the generation of any desired shape. [35]

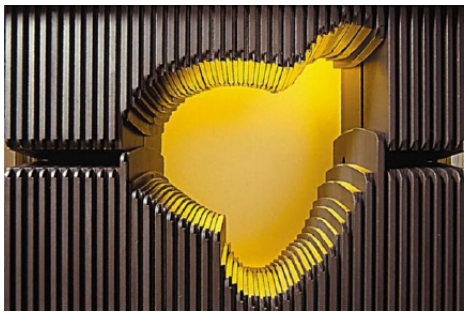

Figure 4.12: Multileaf collimator. Image taken from [35].

With simplified geometry in FLUKA, it has been realized a set of simulations for different thicknesses of the aluminium collimator to mimic the MLC for VHEE electron beams. The choice of aluminium, instead of tungsten or other high Z material, is due to reduce the risk of induced radioactivity in the collimator. Instead of a phantom, a water block was used. In the middle of the aluminium collimator, a square hole of 2x2 cm was placed. The geometry is build in air. The positioning of the electron beam, aluminium collimator, and water can be seen in Fig. 4.13. Electron beam parameters are summarized in Table 4.4. For every thickness of the aluminium collimator, 40 000 primaries per cycle for a total of 3 cycles were generated. The dose distribution can be seen in Fig. 4.16 reference simulation with the beam without MLC and flat beam have been run as well. The cross-section at the beginning of the water block with reference is plotted in Fig. 4.14 and for all of the different thicknesses in Fig. 4.15. It is clear that by increasing the thickness of the aluminium collimator, the dose is more focused on the propagation direction. The goal of this simulation is to determine how thick has to be the aluminium collimator to lower the dose exceeding the hole to less than 10%. This value has not been reached even for a 1 m thick aluminium collimator. Further improvements to these simulations were thus abandoned.

Beam shape	Gaussian
Electron energy	120 MeV
Momentum spread type	Gaussian
Momentum spread FWHM	0.23 GeV/c
FWHM	2 cm
Divergence	10 mrad

Table 4.4: Electron beam parameters.

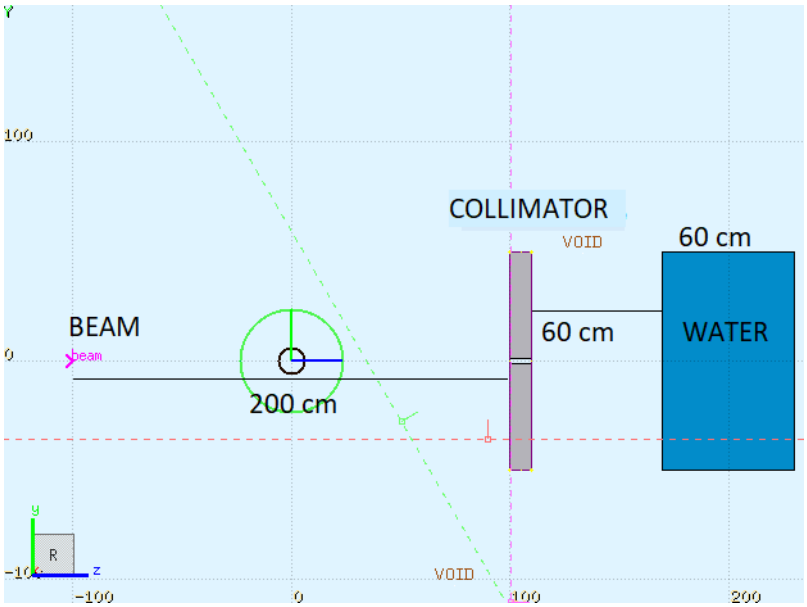

Figure 4.13: Positioning of the beam, shield and water.

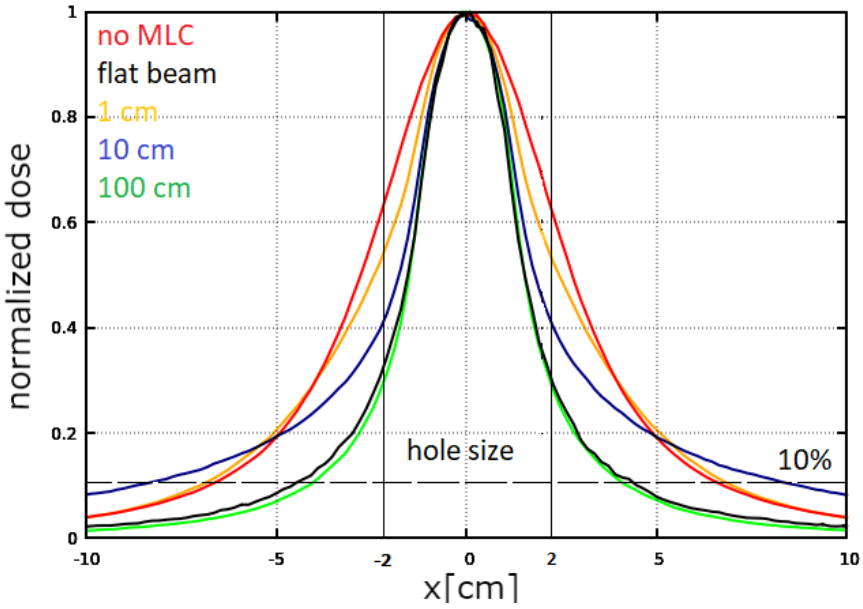

Figure 4.14: Cross section of water phantom.

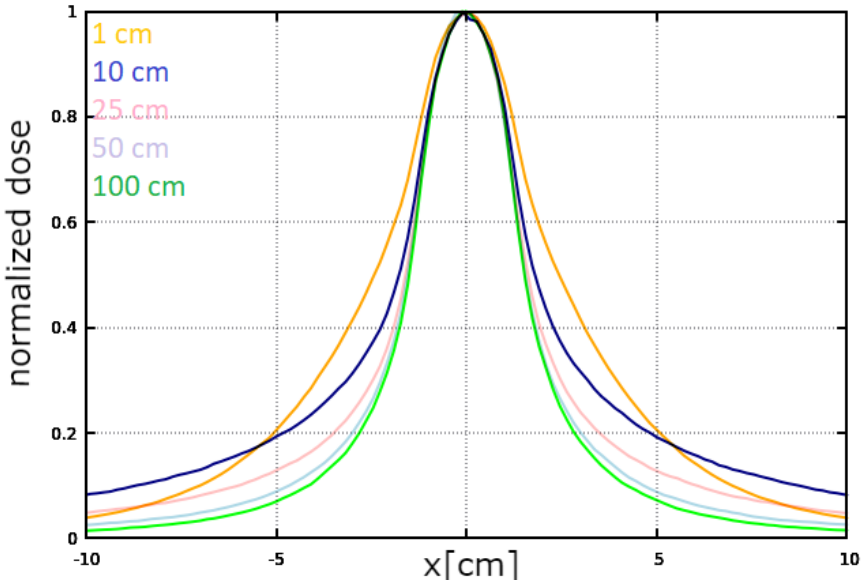

Figure 4.15: Cross section of water phantom with all of the different thicknesses of MLC.

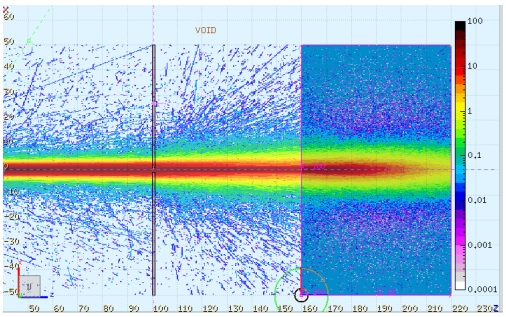

(a) 1 cm thick aluminium collimator.

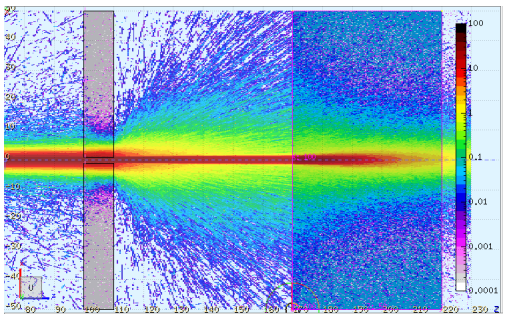

(b) 10 cm thick aluminium collimator.

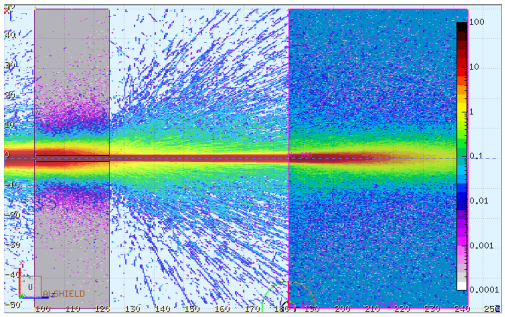

(c) 25 cm thick aluminium collimator.

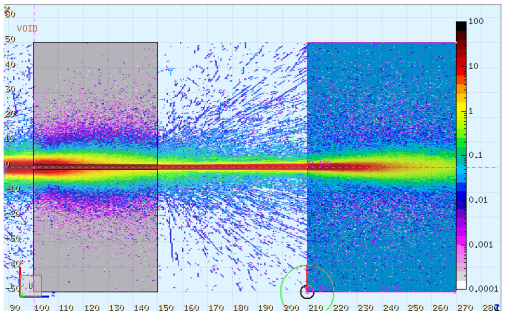

(d) 50 cm thick aluminium collimator.

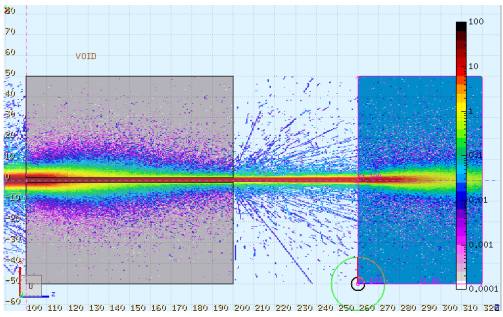

(e) 100 cm thick aluminium collimator.

Figure 4.16: Dose deposition in aluminium collimator for different thickness.

Chapter 5

Laser electron acceleration experiment

The experiment took place in ELI Beamlines in laser hall L1 from November 2021 untill February 2022. The laser system Allegra is being developed by the laser team at ELI Beamlines, it is designed to generate sub-20 fs pulses with energy exceeding 200 mJ with a repetition rate of 1 kHz. The laser is based on the amplification of pulses with OPCPA consisting of a total of seven amplifiers. Allegra laser system has three main blocks: the front end, the booster, and the main amplifier. Schematics of the laser system can be seen in Fig. 5.1. [36]

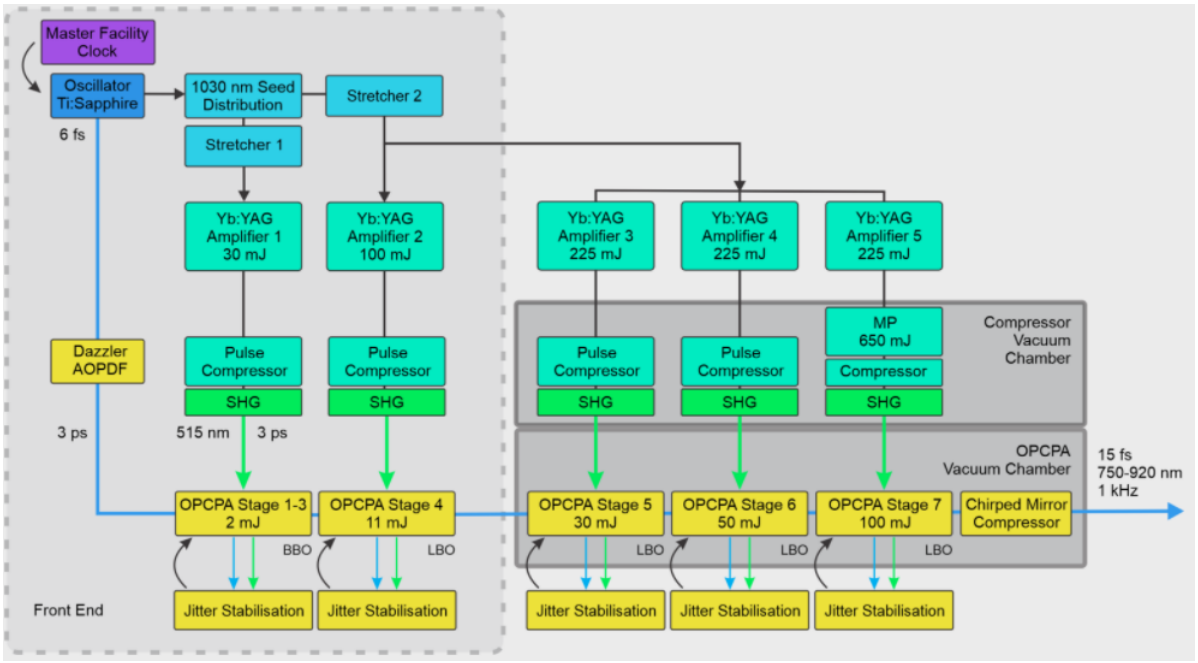

Figure 5.1: Block diagram of L1 Allegra system structure. Image taken from [36].

Designed and actual parameters of the laser system are written in the Table 5.1:

	Designed parameters	Actual parameters
Output pulse energy	100 mJ	30 mJ
Pulse duration	<20 fs	15 fs
Repetition rate	1 kHz	1kHz
Central wavelength	830 < λ< 860 nm	750-λ-920 nm
Beam format	circular, Gaussian-like	circular, Gaussian-like
Beam diameter	27.5 mm at 1/e2	27.5 mm at 1/e2

Table 5.1: L1 Allegra laser system parameters.

The setup of the experiment inside the vacuum chamber of size 70 x 70 cm is shown in Fig. 5.2. Magnet and gas jet nozzle are mounted on a moveable stand to allow scanning in the vacuum. In front of the magnet, an aperture can be installed in order to filter low-energy electrons and improve diagnostics of the beam. Outside the vacuum chamber, several diagnostics are installed as well. For the shadowgraphy of the plasma, a probe beam is used. The water block simulates the head. The gases used in this experiment are nitrogen and a mixture helium and nitrogen.

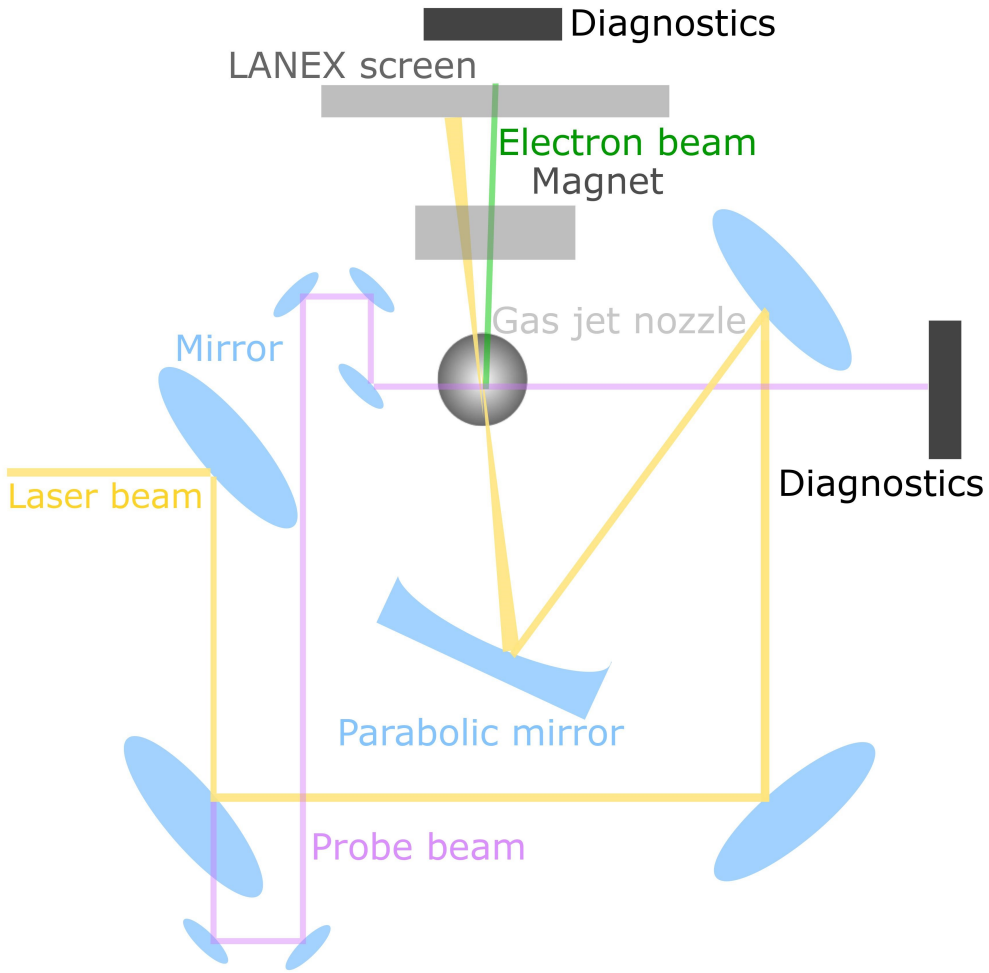

Figure 5.2: Experimental setup of Alfa experiment at ELI Beamlines.

5.1 Electron spectrometer simulation

Simplified geometry of the experiment has been built in FLUKA, to confirm results of how the magnet with aperture will deflect and cut electrons of energy 3, 5, and 7 MeV. These were the energies that were expected in the design phase of the experiment. Actually, during the experimental run, electron beams with energy exceeding 20 MeV have been accelerated. The geometry contains a vacuum chamber, electron beam, magnet, 2 aluminium apertures, LANEX screen, chamber window, water block, and outer aluminium chamber. The electron beam parameters used for the simulations are summarized in Table 5.2.

Energy	3-7 MeV
Divergence	50 mrad
FWHM	0.1 cm
Momentum spread FWHM	7 MeV/c

Table 5.2: Electron beam parameters obtained from the experiment.

In Fig. 5.4, 5.5 and 5.6 electron fluence with logarithmic scale is shown. Magnetic field in the magnet is simplified with magnetic field equal to B=0.1 T. Apertures used for filtration low energy electron are made from aluminium. First aperture is 5 mm thick with 5 mm hole and the second one is 2 mm thick with 1 mm hole. From Fig. 5.4c, 5.5c and 5.6c aperture beam shaping is clear. From Fig. 5.4a, 5.5a and 5.6a deflection of the electron beam due to magnetic field is clear as well.

LANEX screen in the experiment is situated approximately 10 cm behind the magnet. Therefore cross-section plot of electron fluence has been created and is shown in Fig. 5.7. For better comparison cross-section of the beam not influenced by the magnetic field is added. As was expected, lower energy electrons are deflected more than higher-energy electrons. The simulation confirmed expected results.

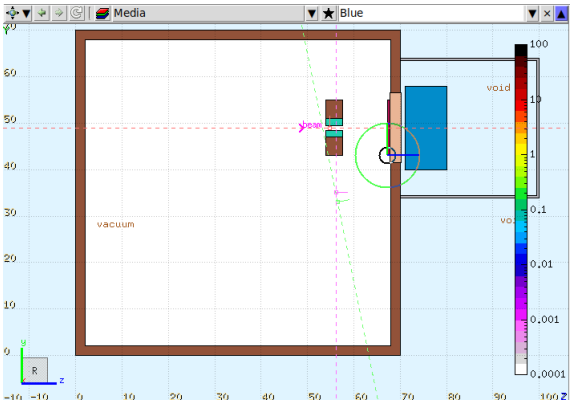

(a) YZ plane.

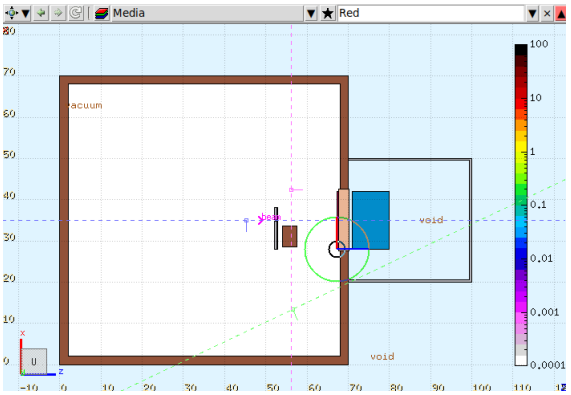

(b) XZ plane.

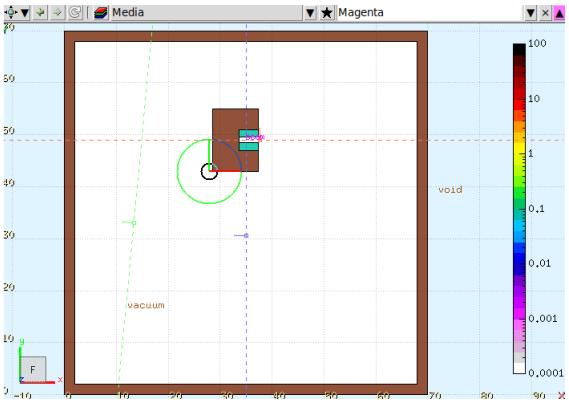

(c) XY plane.

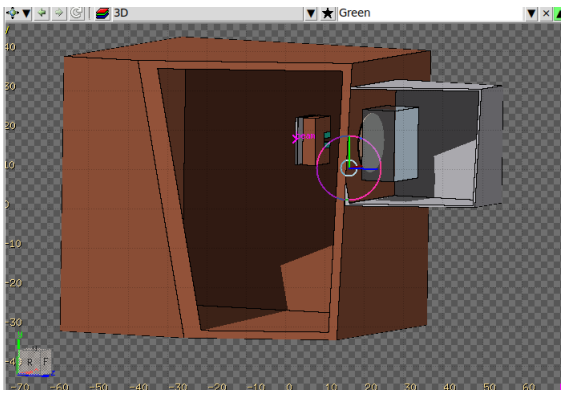

(d) 3D view.

Figure 5.3: Simplified geometry of the experiment in FLUKA.

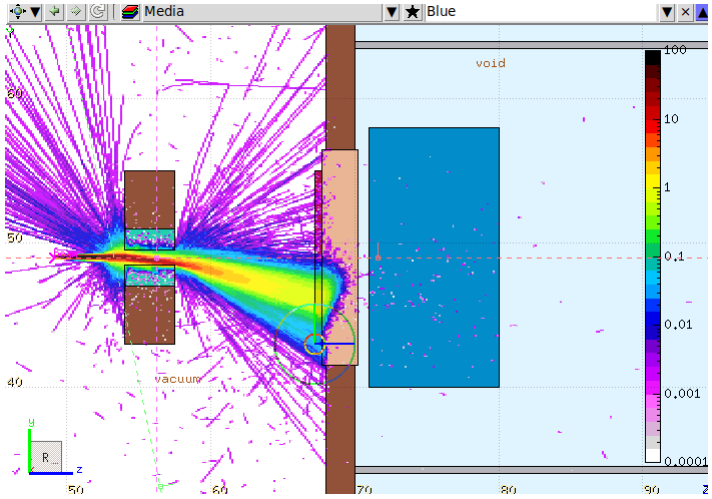

(a) YZ plane.

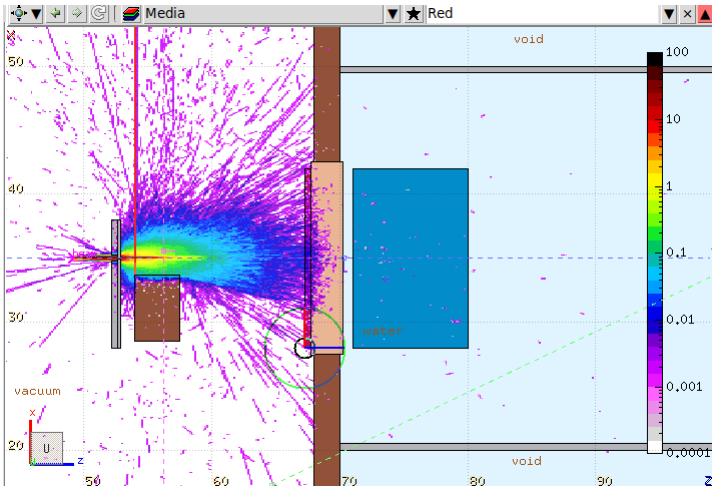

(b) XZ plane.

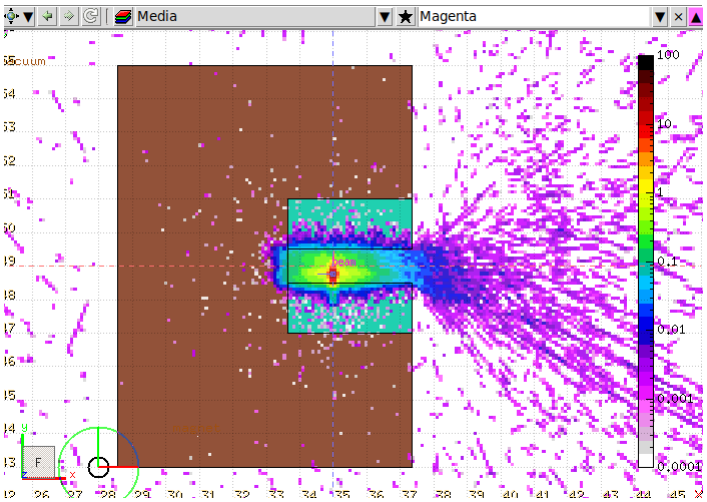

(c) XY plane.

Figure 5.4: Plot of electron fluence with electron energy 3 MeV.

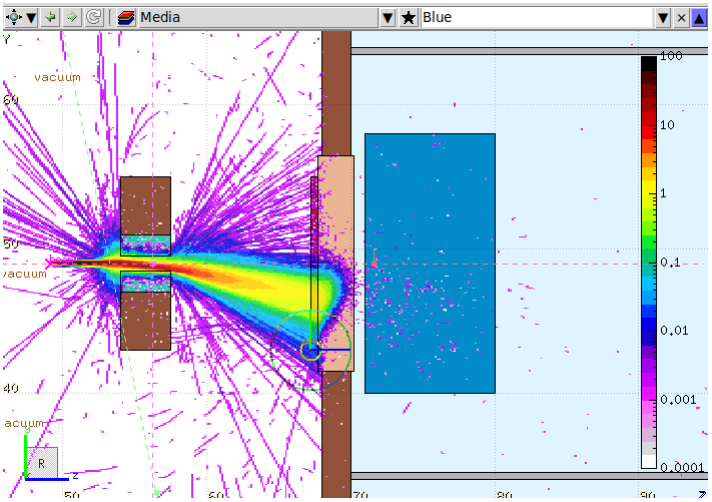

(a) YZ plane.

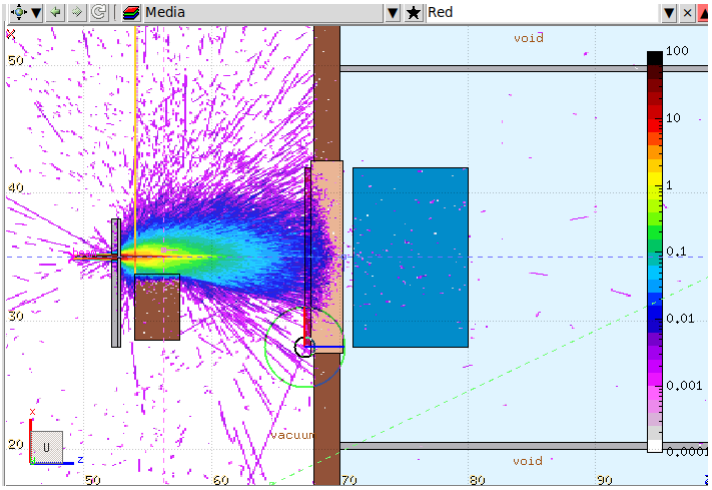

(b) XZ plane.

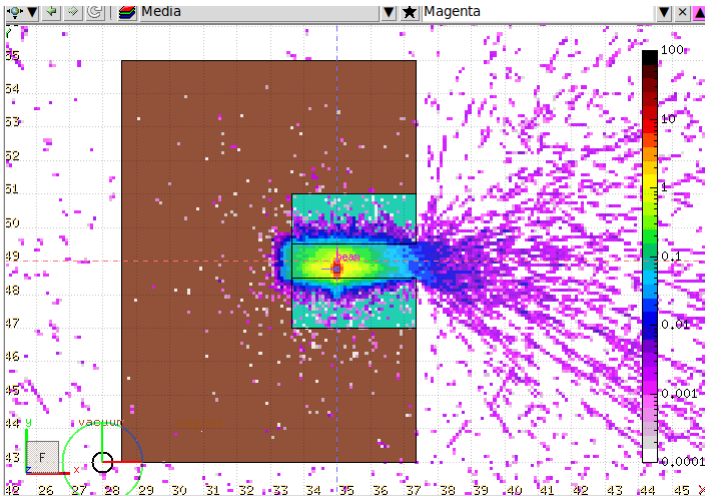

(c) XY plane.

Figure 5.5: Plot of electron fluence with electron energy 5 MeV.

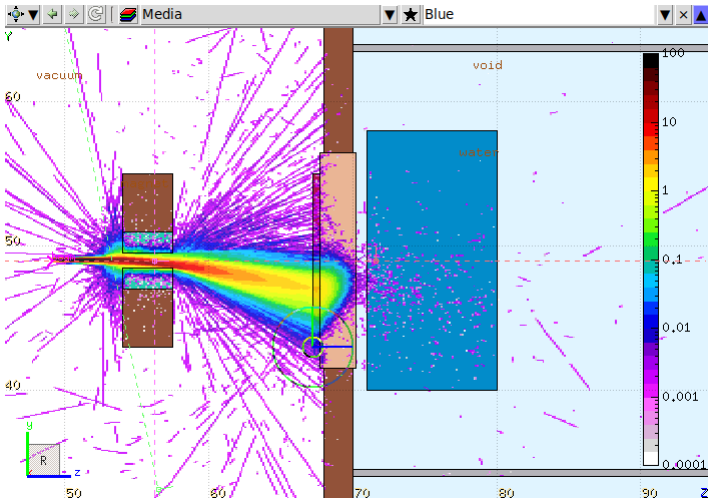

(a) YZ plane.

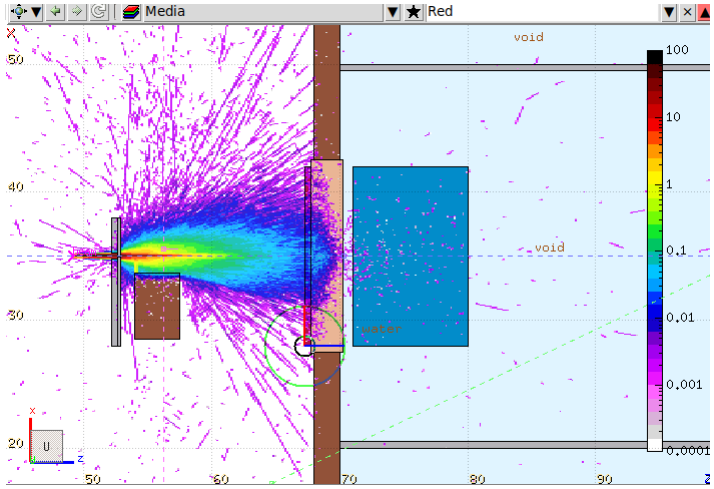

(b) XZ plane.

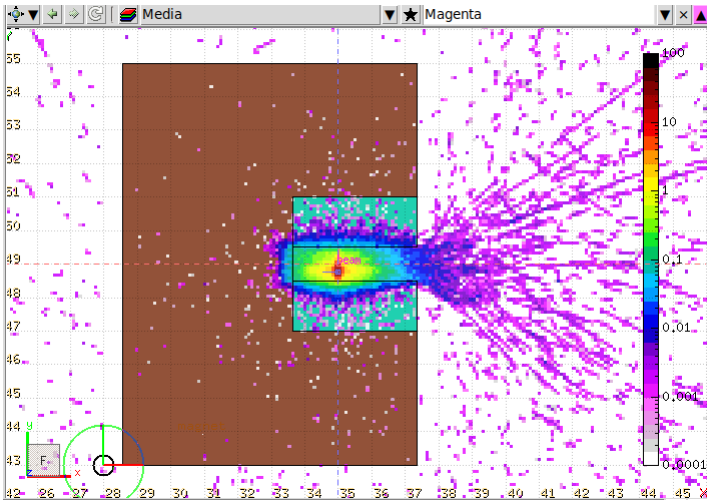

(c) XY plane.

Figure 5.6: Plot of electron fluence with electron energy 6 MeV.

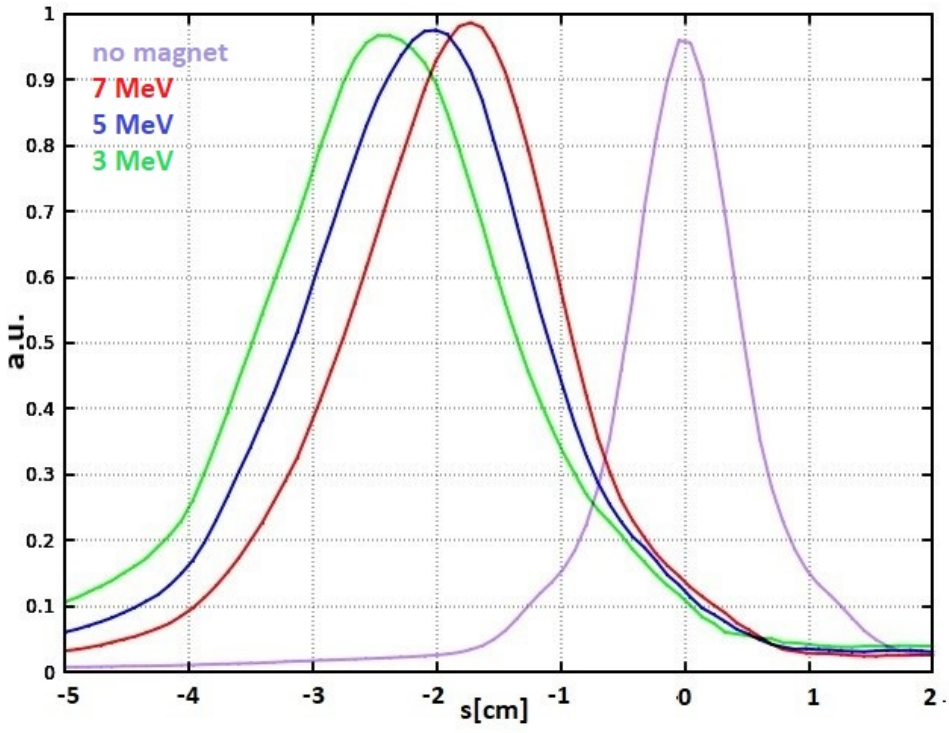

Figure 5.7: Cross-section of electron fluence in Y axis 10 cm behind magnet.

Discussion and conclusion

The purpose of this diploma thesis was to optimize the radiotherapy treatment plan for laser-driven VHEE radiotherapy, compare this type of radiotherapy to other approaches and help with the associated experiment in ELI Beamlines. At the beginning of this work (Chapter 1), laser-plasma accelerators have been examined and a short review was written. Firstly the physical aspects of these accelerators have been described in section 1.1, following the introduction of different regimes in section 1.3 and lastly different techniques for controlling the electron injection and trapping of these electrons were studied in section 1.4.

Chapter 2 starts with the medical motivations of VHEE. In this part, a question as to why are very high electrons studied in correlations to radiotherapy is answered. Succeeding is an analogy of the creation of VHEE with radiofrequency technology and with laser-plasma accelerators. The studies and experiments concluded by scientists all over the world concerning this issue are presented as well.

Detailed description of the methods used in the simulation is situated in Chapter 3. The FLUKA Monte Carlo code and its graphical interface Flair are introduced. After that CT scan of the patient diagnosed with brain cancer, the approximation of the PTV volume, and properties of the electron beams used in the simulation are presented namely in sections 3.2, 3.3 and 3.4.

Subsequently Chapter 4 is dedicated to radiotherapy treatment planning. In section 4.1 positioning of the phantom versus the time of the treatment is studied. The position of the phantom was changed 100 times to properly cover PTV with radiation. A comparison of treatment with 10, 50, and 100 positions and different combination of parameters is conducted. From the results of the simulations is obvious that the case with 100 positions irradiates PTV the best. Nevertheless, the time of the treatment had to be considered as well. With 100 positions time to deliver integrated dose order of 10 Gy is going to take approximately 136 seconds. These results are promising since speed is one of the crucial advantages of treatment with VHEE as opposed to conventional radiotherapy treatment. Further improvement of the treatment that would lead to better coverage is needed. It is desirable to achieve good coverage results in a short amount of time.

Section 4.2 shows that the simulation created in this work can be utilized to study positron radiotherapy treatment. Moreover, the laser-plasma electron accelerator can be as well used to create positrons suitable for positron radiotherapy treatment. This section brings to light the multi-functionality of the simulation and the device currently under development at ELI Beamlines. It has been investigated a treatment planning based on positron beams with kinetic energy comparable with the one of VHEE electrons.

Multileaf collimator has been examined in section 4.3. MLC is used when the size of the beam exceeds the size of the PTV and thus has to be shaped to avoid undesirable exposure to

healthy tissue. Due to dissatisfactory results, it has been decided to abandon this direction of beam shaping.

In the last Chapter 5 experiment conducted in ELI Beamlines is presented. This experiment is conducted with sub-20 fs pulses from the L1 Allegra laser system. It mainly focuses on the generation of the high-energy electron beam. In addition to the simulations that have already been conducted based on the results of the experiment, it is needed to simulate a radiotherapy treatment plan with experimentally obtained electron beam parameters. The obtained electron spectra present a quasi-monoenergetic peak along with a non negligible amount of lower energy electrons. These electrons are undesirable in radiotherapy since they will deposit dose only on the skin of the patient. To solve this problem, magnets can be used to filter low energy electrons. For this reason several simulations with simplified geometry have been conducted in Section 5.1 to deepen the understanding of the results from the diagnostics. This study focuses on the bending of low energy electron beams by magnetic field. It has beeen shown that with increasing energy of the electrons, the influence of the magnetic field on the direction of the electron beam is decreasing.

In this work the basic principles for developing a treatment planning with laser driven VHEE radiation beams are presented and discussed. This work lays the basis for future start-to-end simulations of treatment planning including a realistic description of the laser-driven electron source, optimized magnetic transport, and realistic patient positioning solution.

In conclusion all the tasks of the diploma thesis assignment have been performed. All results from the simulation and experiment are reported.

Bibliography

[1] T. Tajima and J. M. Dawson: *Laser Electron Accelerator*, Phys. Rev. Lett. **43**, 267 (1979)

[2] J. Faure, Y. Glinec, A. Pukhov, S. Kiselev, S. Gordienko, E. Lefebvre, J.P. Rousseau, F. Burgy, V. Malka: *A laser–plasma accelerator producing monoenergetic electron beams*, Nature **431**, 541-544 (2004)

[3] C. G. R. Geddes, Cs. Toth, J. van Tilborg, E. Esarey, C. B. Schroeder,D. Bruhwiler, C. Nieter, J. Cary, W. P. Leemans: *High-quality electron beams from a laser wakefield accelerator using plasma-channel guiding*, Nature **431**, 538-541 (2004)

[4] W. P. Leemans, B. Nagler, A. J. Gonsalves, Cs. Tóth, K. Nakamura, C. G. R. Geddes, E. Esarey, C. B. Schroeder, S. M. Hooker: *GeV electron beams from a centimetre-scale accelerator*, Nature Physics **2**, 696-699 (2006)

[5] S.P.D. Mangles, C.D. Murphy, Z. Najmudin, A.G.R. Thomas, J.L. Collier, A.E. Dangor, E.J. Divall, P.S. Foster, J.G. Gallacher, C.J. Hooker, D.A. Jaroszynski, A.J. Langley, W.B. Mori, P.A. Norreys, F.S. Tsung, R. Viskup, B.R. Walton, K. Krushelnick,*Monoenergetic beams of relativistic electrons from intense laser–plasma interactions*, Nature **431**, 535–538 (2004)

[6] John M. Dawson: *Nonlinear Electron Oscillations in a Cold Plasma*, Physical Review **113**, 383 (1959)

[7] A.J. Gonsalves, K. Nakamura, J. Daniels, C. Benedetti, C. Pieronek, T.C.H. de Raadt, S. Steinke, J.H. Bin, S.S. Bulanov, J. van Tilborg, C.G.R. Geddes, C.B. Schroeder, Cs. Tóth, E. Esarey, K. Swanson, L. Fan-Chiang, G. Bagdasarov, N. Bobrova, V. Gasilov, G. Korn, P. Sasorov, and W.P. Leemans: *Petawatt Laser Guiding and Electron Beam Acceleration to 8 GeV in a Laser-Heated Capillary Discharge Waveguide* Physical Review **122**, 084801 (2019)

[8] O. Lundh, J. Lim, C. Rechatin, L. Ammoura, A. Ben-Ismaïl, X. Davoine, G. Gallot, J-P. Goddet, E. Lefebvre, V. Malka, J. Faure: *Few femtosecond, few kiloampere electron bunch produced by a laser–plasma accelerator* Nature Physics **7**, 219-222 (2011)

[9] A.R. Maier, N. M. Delbos, T. Eichner, L. Hübner, S. Jalas, L. Jeppe, S. W. Jolly, M. Kirchen, V. Leroux, P. Messner, M. Schnepp, M. Trunk, P.A. Walker, Ch. Werle, P. Winkler: *Decoding Sources of Energy Variability in a Laser-Plasma Accelerator*, Physical Review **10**, 031039 (2020)

[10] I. Kostyukov, A. Phukov, S. Kiselev: *Phenomenological theory of laser-plasma interaction in "bubble" regime*, Physics of Plasmas **11**, 5256 (2004)

[11] S.M.Hooker: *Developments in laser-driven plasma accelerators*, Nature Photonics **7**, 775-782 (2013)

[12] S. Corde, K. Ta Phuoc, G. Lambert, R. Fitour, V. Malka, A. Rousse: *Femtosecond x rays from laser-plasma accelerators*, Reviews of modern physics **85**, 1 (2013)

[13] A. Modena, Z. Najmudin, A. E. Dangor, C. E. Clayton, K. A. Marsh, C. Joshi, V. Malka, C. B. Darrow, C. Danson, D. Neely, F. N. Walsh: *Electron acceleration from the breaking of relativistic plasma waves*, Nature **377**, 606-608 (1995)

[14] V. Malka: *Laser plasma accelerators*. Physics of Plasmas **5**, 055501 (2012)

[15] J. Faure, C. Rechatin, A. Norlin, A. Lifschitz, Y. Glinec, V. Malka: *Controlled injection and acceleration of electrons in plasma wakefields by colliding laser pulses*, Nature **444**, 737-739 (2006)

[16] S. Bulanov, N. Naumova, F. Pegoraro, J. Sakai: *Particle injection into the wave acceleration phase due to nonlinear wake wave breaking*, Physical Review **58**, R5257 (1998)

[17] C. McGuffey, A.G.R. Thomas, W. Schumaker, T. Matsuoka, V. Chvykov, F.J. Dollar, G. Kalintchenko, V. Yanovsky, A. Maksimchuk, K. Krushelnick, V. Yu. Bychenkov, I.V. Glazyrin, A.V. Karpeev: *Ionization Induced Trapping in a Laser Wakefield Accelerator*, Physical Review **104**, 025004 (2010)

[18] A. Pak, K.A. Marsh, S.F. Martins, W. Lu, W.B. Mori, C. Joshi, *Injection and Trapping of Tunnel-Ionized Electrons into Laser-Produced Wakes*, Physical Review **104**, 025003 (2010)

[19] C. Thaury, E. Guillaume, A. Lifschitz, K. Ta Phuoc, M. Hansson, G. Grittani, J. Gautier, J.-P. Goddet, A. Tafzi, O. Lundh, V. Malka: *Shock assisted ionization injection in laser-plasma accelerators*, Scientific Reports **5**, 16310 (2015)

[20] C. M. DesRosiers, V. Moskvin, A.F. Bieljaw and L. Papiez: *150-250 MeV electron beams in radiation therapy*, Phys. Med. Biol. **45**,) 1781–1805 (2000)

[21] M. Bazalova-Carter, B.Qu, B. Palma, B. Hårdemark and E. Hynning, Ch. Jensen, P. G. Maxim, and B. W. Loo, Jr.: *"Treatment planning for radiotherapy with very high-energy electron beams and comparison of VHEE and VMAT plans"*, Medical Physics, **42**, 2615-2625 (2015)

[22] L. Whitmore, R. I. Mackay, M. van Herk, J. K. Jones, R. M. Jones: *Focused VHEE (very high energy electron) beams and dose delivery for radiotherapy applications*, Scientific Reports **11**, (2021)

[23] P. G. Maxim, S. G. Tantawi, B. W. Loo Jr.: *PHASER: A platform for clinical translation of FLASH cancer radiotherapy*, Radiotherapy and Oncology **139**, 28 (2019)

[24] C. M. DesRosiers, V. Moskvin, M. Cao, C. Joshi: *"Laser-plasma generated very high energy electrons in radiation therapy of the prostate"*, Proceedings of SPIE - The International Society for Optical Engineering **6881**, , 688109 (2008)

[25] A. Subiel, V. Moskvin, G.H. Welsh, S. Cipiccia, D. Reboredo, P. Evans, M. Partridge, C. DesRosiers, M.P. Anania, A. Cianchi, A. Mostacci, E. Chiadroni, D. Di Giovenale, F. Villa, R. Pompili, M. Ferrario, M. Belleveglia, G. Di Pirro, G. Gatti, C. Vaccarezza, B. Seitz, R.C. Isaac, E. Brunetti, S.M. Wiggins, B. Ersfeld, M.R. Islam, M.S. Mendonca, A. Sorensen, M. Boyd, D.A. Jaroszynski: *Dosimetry of very high energy electrons (VHEE) for radiotherapy applications: using radiochromic film measurements and Monte Carlo simulations* Phys. Med. Biol. **59**, 5811–5829 (2014)

[26] K. Kokurewicz, E. Brunetti, A. Curcio, D. Gamba, L. Garolfi, A. Gilardi, E. Senes, K. N. Sjobak, W. Farabolini, R Corsini, D. A. Jaroszynski: *An experimental study of focused very high energy electron beams for radiotherapy*, Communications Physics **4**, 33 (2021)

[27] E. Schüler, K. Eriksson, E. Hynning, M. Bazalova-Carter, S. L. Hancock, S. M. Hiniker, T. Wong, Q. Le, B. W. Loo Jr., P. G. Maxima: *"Very high-energy electron (VHEE) beams in radiation therapy; Treatment plan comparison between VHEE, VMAT, and PPBS"*, Medical Physics **44**, 6 (2017)

[28] A. Subiel, V. Moskvin, G. H. Welsh, S. Cipiccia, D. Reboredo, C. DesRosiers, D. A. Jaroszynski: *Challenges of dosimetry of ultra-short pulsed very high energy electron beams*, Physica Medica **42**, 327-331 (2017)

[29] T. Fuchs, H. Szymanowski, U. Oelfke, Y. Glinec, C. Rechatin, J. Faure, V. Malka: *Treatment planning for laser-accelerated very-high energy electrons*, Phys. Med. Biol.**54**, 11 (2009)

[30] C. Ahdida, D. Bozzato, D. Calzolari, F. Cerutti, N. Charitonidis, A. Cimmino, A. Coronetti, G. L. D'Alessandro, A. Donadon Servelle, L. S. Esposito, R. Froeschl, R. García Alía, A. Gerbershagen, S. Gilardoni, D. Horváth, G. Hugo, A. Infantino, V. Kouskoura, A. Lechner, B. Lefebvre, G. Lerner, M. Magistris, A. Manousos, G. Moryc, F. Ogallar Ruiz, F. Pozzi, D. Prelipcean, S. Roesler, R. Rossi, M. Sabaté Gilarte, F. Salvat Pujol, P. Schoofs, V. Stránský, C. Theis, A. Tsinganis, R. Versaci, V. Vlachoudis, A. Waets, M. Widorski, *New Capabilities of the FLUKA Multi-Purpose Code*, Frontiers in Physics **9**, 788253 (2022)

[31] V. Vlachoudis, *FLAIR: A Powerful But User Friendly Graphical Interface For FLUKA*, Proc. Int. Conf. on Mathematics, Computational Methods Reactor Physics (MC 2009), Saratoga Springs, New York (2009)

[32] T. Hioki, Y. H. Gholami, K. J. McKelvey, A. Aslani, H. Marquis, E. M. Eslick, K. P. Willowson, V. M. Howell, D. L. Bailey: *Overlooked potential of positrons in cancer therapy*, Scientific Reports **11**, 2475 (2021)

[33] G. Sarri et al., *Generation of neutral and high-density electron–positron pair plasmas in the laboratory* Nat. Commun. **6**, 6747 (2015)

[34] J. Couperus et al., *Demonstration of a beam loaded nanocoulomb-class laser wakefield accelerator*, Nat. Commun. **8**, 487 (2017)

[35] M. Jeraj, V. Robar *Multileaf collimator in radiotherapy*, Radiol. Oncol **38**, 235-240 (2004)

[36] `https://www.eli-beams.eu/cs/infrastruktura/lasery/laser-1-allegra-100-mj-1-khz/`, 20.4.2022